Available online at www.sciencedirect.com
ScienceDirect
Geochimica et Cosmochimica Acta 72 (2008) 5090–5110
Geochimica et Cosmochimica Acta
www.elsevier.com/locate/gca

Sulfur in peridotites and gabbros at Lost City (30°N, MAR): Implications for hydrothermal alteration and microbial activity during serpentinization

Adélie Delacour [a,*,1], Gretchen L. Früh-Green [a], Stefano M. Bernasconi [b], Deborah S. Kelley [c]

[a] Institute for Mineralogy and Petrology, ETH Zurich, CH-8092 Zurich, Switzerland
[b] Geological Institute, ETH Zurich, CH-8092 Zurich, Switzerland
[c] School of Oceanography, University of Washington, Seattle, WA 98195, USA

Received 14 June 2008; accepted in revised form 23 July 2008; available online 6 August 2008

Abstract

Variations in sulfur mineralogy and chemistry of serpentinized peridotites and gabbros beneath the Lost City Hydrothermal Field at the southern face of the Atlantis Massif (Mid-Atlantic Ridge, 30°N) were examined to better understand serpentinization and alteration processes and to study fluid fluxes, redox conditions, and the influence of microbial activity in this active, peridotite-hosted hydrothermal system. The serpentinized peridotites are characterized by low total sulfur contents and high bulk $\delta^{34}S$ values close to seawater composition. Low concentrations of ^{34}S-enriched sulfide phases and the predominance of sulfate with seawater-like $\delta^{34}S$ values indicate oxidation, loss of sulfide minerals and incorporation of seawater sulfate into the serpentinites. The predominance of pyrite in both serpentinites and gabbros indicates relatively high fO_2 conditions during progressive serpentinization and alteration, which likely result from high fluid fluxes during hydrothermal circulation and evolution of the Lost City system from temperatures of ~250 to 150 °C. Sulfate and sulfide minerals in samples from near the base of hydrothermal carbonate towers at Lost City show $\delta^{34}S$ values that reflect the influence of microbial activity. Our study highlights the variations in sulfur chemistry of serpentinized peridotites in different marine environments and the influence of long-lived, moderate temperature peridotite-hosted hydrothermal system and high seawater fluxes on the global sulfur cycle.

1. INTRODUCTION

Only five of the known hydrothermal sites located between 10° and 40°N along the Mid-Atlantic Ridge (MAR), Rainbow, Logatchev, Ashadze, Lost City and Saldanha, are hosted by variable mixtures of serpentinized peridotite and mafic material and are characterized by vent fluid chemistries distinct from those in basaltic environments (e.g., Rona et al., 1987; Krasnov et al., 1995; Donval et al., 1997; Douville et al., 1997; Sagalevich et al., 2000; Holm and Charlou, 2001; Kelley et al., 2001; German and Von Damm, 2003; Baker and German, 2004; Kelley et al., 2005). The discovery of these peridotite-hosted hydrothermal systems has stimulated intense interest in the role of serpentinization in crustal aging processes and global geochemical fluxes in ridge and subduction zone environments. In addition, the production of methane (CH_4), hydrogen (H_2) and various sulfur species during serpentinization is believed to play an important role in sustaining subsurface microbial communities in near-vent environments away from volcanic ridge centers and has important implications for the existence of a deep

* Corresponding author. Fax: +33 1 44 27 99 69.
E-mail address: delacour@ipgp.jussieu.fr (A. Delacour).
[1] Present address: Laboratoire de Géosciences Marines, Institut de Physique du Globe de Paris, 4 place Jussieu, 75252 Paris Cedex 5, France.

0016-7037/$ - see front matter © 2008 Elsevier Ltd. All rights reserved.
doi:10.1016/j.gca.2008.07.017

H_2-based biosphere (Alt and Shanks, 1998; Boetius et al., 2000; Boetius, 2005; Kelley et al., 2005; Brazelton et al., 2006). In turn, microbial activity may have a significant affect on C–H–S cycles in peridotite-hosted hydrothermal systems.

The Lost City Hydrothermal Field (LCHF) is distinctly different from all known marine hydrothermal systems and hosts carbonate-brucite structures up to 60 m in height that are deposited from alkaline fluids emanating from fault zones that tap a region of active serpentinization of underlying peridotites (Kelley et al., 2001, 2005; Ludwig et al., 2006). Serpentinization reactions and cooling of mantle and gabbroic rocks within the massif produce Ca-rich, high pH (9–11) fluids with elevated concentrations of H_2, CH_4, and other low-molecular weight hydrocarbons venting at temperatures of 40–91 °C (Kelley et al., 2005; Proskurowski et al., 2006, 2008). Diffuse flow supports sulfur-oxidizing, sulfate-reducing, and methane-oxidizing bacteria on the exterior of the chimneys, while methanogenic and/or methanotrophic *Archaea* dominate the porous interior walls (Schrenk et al., 2004; Brazelton et al., 2006). These metabolic groups of microorganisms indicate a tight coupling of microbial cycling of S, H_2 and CH_4. Thus, the LCHF represents an ideal opportunity to study sulfur geochemistry and sulfur cycling in an active serpentinite-driven hydrothermal system and to evaluate linkages between seawater–rock interaction, redox conditions, and microbial activity.

Sulfur in seafloor hydrothermal systems has two main sources with distinct isotopic signatures: sulfide of mantle origin with a $\delta^{34}S$ value of $+0.1 \pm 0.5‰$ (Sakai et al., 1984; Alt et al., 1989; Shanks et al., 1995; Shanks, 2003) and seawater sulfate with a $\delta^{34}S$ value of $+21‰$ (Rees et al., 1978). Redox reactions and mixing of sulfur sources in hydrothermal systems influence the S-isotope compositions of the rocks, fluids, and sulfide deposits, and have consequences for the global sulfur cycle over time (Alt, 1994; Shanks et al., 1995; Alt and Shanks, 2003). Sulfur contents and isotope variability in hydrothermal systems are also influenced by inorganic production of H_2S and by biogenic sulfate reduction. Microbial reduction of seawater sulfate typically produces sulfide phases with $\delta^{34}S$ values of $-40‰$ to $-10‰$ (Goldhaber and Kaplan, 1980; Brunner and Bernasconi, 2005); and similar compositions in oceanic serpentinites have been attributed to such processes (Alt and Shanks, 1998).

Sulfur isotope studies on high-temperature black smoker systems along the MAR, e.g., Logatchev (Bogdanov et al., 1997; Eickmann et al., 2005, 2006) and Lucky Strike (Rouxel et al., 2004), and on serpentinized oceanic peridotites and lower crustal gabbros from different spreading and tectonic environments [Hess Deep and Iberian Margin (Alt and Shanks, 1998), MARK area (Alt and Shanks, 2003), Hole 735B (Alt and Anderson, 1991), Mariana arc (Alt and Shanks, 2006), 15°20'N (Alt et al., 2007)], show that a magmatic source of sulfur is dominant in basalt-hosted systems. In contrast, large variations in sulfur speciation, content and isotope composition characterize oceanic serpentinites.

Here we present a study of the sulfur mineralogy, sulfur content and S-isotope compositions of serpentinized peridotites and gabbros that form the southern face of the Atlantis Massif beneath the Lost City hydrothermal system. We compare these data with other results from black smoker systems, oceanic serpentinites and gabbros (Table 1) and with studies of a lower crustal gabbroic sequence drilled at the central dome of the Atlantis Massif, 5 km north of the LCHF (Delacour et al., this issue). In addition, we discuss abiogenic and/or biogenic processes and changes in sulfur content and speciation associated with serpentinization and conclude that high seawater fluxes are coupled with increases in oxygen and sulfur fugacities and that they have important consequences for the sulfur mineralogy and sulfur geochemistry of this system.

2. THE ATLANTIS MASSIF

Over the last ten years the Atlantis Massif (AM) has been the target of a number of field and laboratory investigations. This 1.5–2 Myr-old dome-like massif is located at 30°N, 15 km west of the MAR axis at the intersection with the Atlantis Transform Fault (ATF, Fig. 1a) and is interpreted as an oceanic core complex (OCC; Cann et al., 1997; Blackman et al., 1998, 2002). The morphology of the AM is characterized by three components: the gabbroic central dome, the peridotite-dominated southern ridge, and the volcanic eastern block, which is considered the hanging wall of the OCC (Fig. 1a; Blackman et al., 2002; Karson et al., 2006).

2.1. The central dome

The central dome of the AM is marked by corrugations and striations on its surface, which are believed to be traces of a low-angle, long-lived detachment fault that led to the uplift and exposure of the massif (Cann et al., 1997; Blackman et al., 2002; Karson et al., 2006; Ildefonse et al., 2007). Results from the Integrated Ocean Drilling Program (IODP) at Site U1309 (Expeditions 304 and 305) show that the central dome is mainly composed of gabbroic rocks (91.4% total recovery) with minor intercalated ultramafic lithologies (Expedition Scientific Party, 2005a,b; Blackman et al., 2006). Mineral assemblages in the core from Hole 1309D [drilled to a depth of 1415.5 m below sea floor (mbsf)] record a cooling and alteration history from magmatic to zeolite facies conditions (Expedition Scientific Party, 2005a,b; Blackman et al., 2006). However, greenschist metamorphic conditions (<500 °C) were dominant in the central dome and only minor deformation under granulite-amphibolite conditions are recorded in the gabbroic rocks. This suggests that deformation related to the detachment faulting was not recovered or that it occurred at lower temperatures than at the southern wall (Schroeder and John, 2004). The degree of alteration decreases downhole and the presence of local zeolite veins below 700 mbsf is related to late-stage fracturing and seawater penetration along faults.

Table 1
Locations and sulfur isotope compositions of fluids and sulfide minerals from black smoker systems, and of oceanic serpentinites and gabbros from various tectonic settings

Name	Location	Hydrothermal system	Temperature of fluids	Basement rocks	Mineral assemblages	$\delta^{34}S_{sulfide}$	$\delta^{34}S_{sulfate}$	References
Black smoker basalt-hosted hydrothermal systems								
EPR	21°N, Pacific	Black smoker	380 °C ± 30 °C	Basalts		+1.4‰ to +3.0‰		Arnold and Sheppard (1981)
			260–350 °C		wu, cpy, py, cu + anh	+1.3‰ to +4.1‰	+19.6‰ to +20.8‰	Styrt et al. (1981)
EPR	21°N, Pacific	Black smoker	350 °C	Basalts	Black smoker: sph, py, cpy	+1.8‰ to +1.9‰	anh: +18.96‰	Kerridge et al. (1983)
					Dead chimney: sph, cpy, py, S	−0.4‰ to +3.0‰		
					Basal mound: sph, cpy, py	+1.5‰ to +2.3‰		
					Sediment: po, sph, py	+0.7‰ to +1.3‰		
					Vent fluid	+3.4‰ to +3.7‰		
Juan de Fuca	Pacific	Black smoker	220–284 °C	Basalts	Fluid	+4‰ to +7.4‰		Shanks and Seyfried (1987)
					Chimney sulfides: sph, cpy, isocu, po	+1.6‰ to +5.7‰	+20.4‰ to +21.4‰	
Galapagos Rift	85° 55′W	Black smoker	Low *T* (17 °C)	Basalts	cpy, py /source of sulfur: sw	+5.4‰ to +6.3‰		Skirrow and Coleman (1982)
					cpy, py ± ma, sph, ga, ba	+2.7‰ to +5.5‰		Knott et al. (1995)
TAG	26° 08′N, MAR		360–366 °C / 273–301 °C	Pillow lavas/ Basalts	py, cpy, anh	+6.5‰ to +8.8‰	+21.4‰ to +22.8‰	Chiba et al. (1998)
					py, cpy, sph, anh (stockwork zone)	+0.3‰ to +10.2‰	+20.5‰ to +21.5‰	Gemmel and Sharpe (1998)
					py, ma, sph, cpy, anh (vertical section through the mound)	+4.4‰ to +8.9‰	+19.2‰ to +20.9‰	Knott et al. (1998)
Broken Spur	29° 10′N, MAR	Black smoker	357–366 °C	Pillow lavas/ Basalts	ma, py, cpy, sph, wu, isocu, po, anh	−0.8‰ to +2.4‰	+ 19.3‰	Duckworth et al. (1995)
Mariana back arc	18° 13′N	Black smoker	287 °C	Basalts	ba, sph, ga, cpy, py	+2.1‰ to +3.1‰	+21‰ to +22‰	Kusukabe et al. (1990)
					Vent fluids	+3.6‰ to +4.8‰		
Hole 504B	Eastern Pacific			Volcanic section and sheeted dikes	Pillow basalts	−11‰ to +1.6‰	+18.5‰ to +36‰	Alt et al. (1989)
					Transition zone + dikes		~Seawater	
Snake Pit	23° 22′N, MAR	Black smoker	350 °C	Basalts	isocu, py, ma, cpy, sph, po	+1.2‰ to +2.8‰		Kase et al. (1990)
Lucky Strike	37° 17′N, MAR	Black smoker	170–364 °C[b]	Basalts	cpy, py, ma, sph, co, ba, anh	−0.5‰ to +4.6‰	~Seawater	Rouxel et al. (2004)
Hole 735B	Indian Ocean, Atlantis II FZ			Gabbros	po, cpy, pn, tr, py	−3.2‰ to +6.9‰ py: −2.1‰ to +0.8‰	+3.2‰ to +23.5‰	Alt and Anderson (1991)
Serpentinized abyssal peridotites and hydrothermal systems								
Logatchev	14° 45′N, MAR	Black smoker	347–352 °C[b]	Ultramafic rocks	cpy, sph, py, ma, bo	+0.7‰ to +13.8‰		Bogdanov et al. (1997)
					cpy, py, po + anh	+2‰ to +9‰	+ 17.5‰ to +20‰	Eickmann et al. (2005, 2006)

Hess Deep	EPR		Serpentinites (275-375 °C[a])	aw, pn, hz, mi, ma, va	+1.5‰ to −23.7‰	−3.3‰ to +21.5 ‰	Alt and Shanks (1998)
Iberian Margin	41°N, Atlantic		Serpentinites (~20–200 °C[a])	py, mi, va, pn, cpy	−25‰ to −43.7‰	−19.5‰ to +25.1‰	Alt and Shanks (1998)
MARK area	MAR, Kane FZ, 23°N	335–350 °C[b]	Serpentinites + gabbros	pn, po, mi, cpy, ±hz ± aw	+3.7‰ to +12.7‰	+5‰ to +20.3‰	Alt and Shanks (2003)
Mariana and Izu-Bonin arcs	Western Pacific	3 °C	Serpentinites		−6.7‰ to +9.8‰	−20‰ to +30.9‰	Alt and Shanks (2006)
15° 20′N (ODP Leg 209)	MAR		Serpentines + gabbros (<150–350 °C)	pn, cpy, bo, aw, hz, va, py, mi, po, vio	−32.1‰ to +10.8‰	−4.5‰ to +15.3‰	Alt et al. (2007)
IODP Site U1309	Atlantis Massif, 30°N		Gabbros + minor serpentinites	pn, mac, po, mi, py, cpy, hz, vio	−1.5‰ to +13.9‰	+7.3‰ to +22.8‰	Delacour et al. (this issue)
Lost City		40–91 °C[b]	Serpentinites + minor gabbros	py, pn, po, cpy	−22.9‰ to +19.4‰	+3.6‰ to +22‰	This study

Mineral abbreviations: po: pyrrhotite, cpy: chalcopyrite, py: pyrite, pn: pentlandite, hz: heazlewoodite, aw: awaruite, bo: bornite, vio: violarite, mac: mackinawite, mi: millerite, va: valleriite, sph: sphalerite, ma: marcasite, anh: anhydrite, tr: troilite, cu: cubanite, isocu: isocubanite, wu: wurtzite, ga:galena, ba: barite, co: covellite, sw: seawater; S: elemental sulfur.

[a] Temperature range of serpentinization; references Hess Deep (Agrinier et al., 1995), Iberian Margin (Agrinier et al., 1996), 15° 20′N (Alt et al., 2007).

[b] References of hydrothermal fluid temperatures: Logatchev, Lucky Strike and MARK (Charlou et al., 2002), Lost City (Kelley et al., 2001, 2005). References for fluid temperatures of other sites are given in the table.

2.2. The southern wall and the Lost City Hydrothermal Field

Analyses of dredge and submersible samples show that the southern wall of the AM is dominated by serpentinized peridotites (70%) with interspersed smaller bodies of altered gabbroic rocks (30%; Kelley et al., 2001, 2005; Boschi et al., 2006; Karson et al., 2006), in striking contrast to the central dome. A 100 m-thick detachment shear zone (DSZ), composed of highly deformed serpentinized peridotites and lesser metagabbros affected by talc and/or amphibole metasomatism, forms the crest of the massif (Boschi et al., 2006; Karson et al., 2006). This highly deformed metasomatic zone is related to focused fluid flow and strain localization during exhumation of the massif (Schroeder and John, 2004; Boschi et al., 2006). Fossil-rich limestones, chalks, and sedimentary breccias with clasts of serpentinized peridotites, metagabbros and basalts overlie the DSZ and form a flat-lying cap at the top of the massif (Früh-Green et al., 2003; Kelley et al., 2005; Karson et al., 2006). This carbonate cap is strongly lithified and is believed to act as a barrier for heat and fluids emanating from the LCHF (Früh-Green et al., 2003; Kelley et al., 2005).

The LCHF is located on a fault-bounded terrace at water depths of 750–850 m along the south wall of the AM (Kelley et al., 2001) and hosts at least 40 active and inactive carbonate-brucite chimneys that are aligned in an E–W trending direction oblique to the ATF (Fig. 1b). The vent fluids contain 1–2 mmol/kg CH_4 and 1–15 mmol/kg H_2 and have elevated concentrations of other low-molecular weight hydrocarbons (Kelley et al., 2005; Proskurowski et al., 2006, 2008). Most of the carbonate towers are built on or grow directly from the serpentinite basement rocks. Radiocarbon age-dating show that hydrothermal activity at Lost City has been ongoing for at least 30–35 kyr (Früh-Green et al., 2003) and most likely longer (Ludwig et al., 2006). Modeling suggests that the system may have the potential to be active for tens of thousands of years (Lowell and Rona, 2002; Früh-Green et al., 2003).

3. METHODS

3.1. Field sampling

This study is based on mineralogical, petrological and geochemical investigations of >150 samples and is part of an extensive multidisciplinary project aimed at understanding the crustal architecture, alteration history and exhumation of the Atlantis Massif and the formation of the LCHF. The LCHF was discovered during the MARVEL Expedition in 2000 (R/V *Atlantis* cruise AT3-60; Kelley et al., 2001), and 15 *Alvin* dives sampled the central dome and the southern wall (dives 3639 through 3652; Blackman et al., 2002; Schroeder and John, 2004; Boschi et al., 2006; Karson et al., 2006). In 2003, the R/V *Atlantis* (cruise AT7-34) conducted detailed mapping and sampling of the southern wall in the vicinity of the LCHF. Nineteen *Alvin* dives (dives 3862 through 3881) collected co-registered samples of basement rock, vent fluid, vent material, sediment, and micro- and macrofauna (Kelley et al., 2005; Boschi

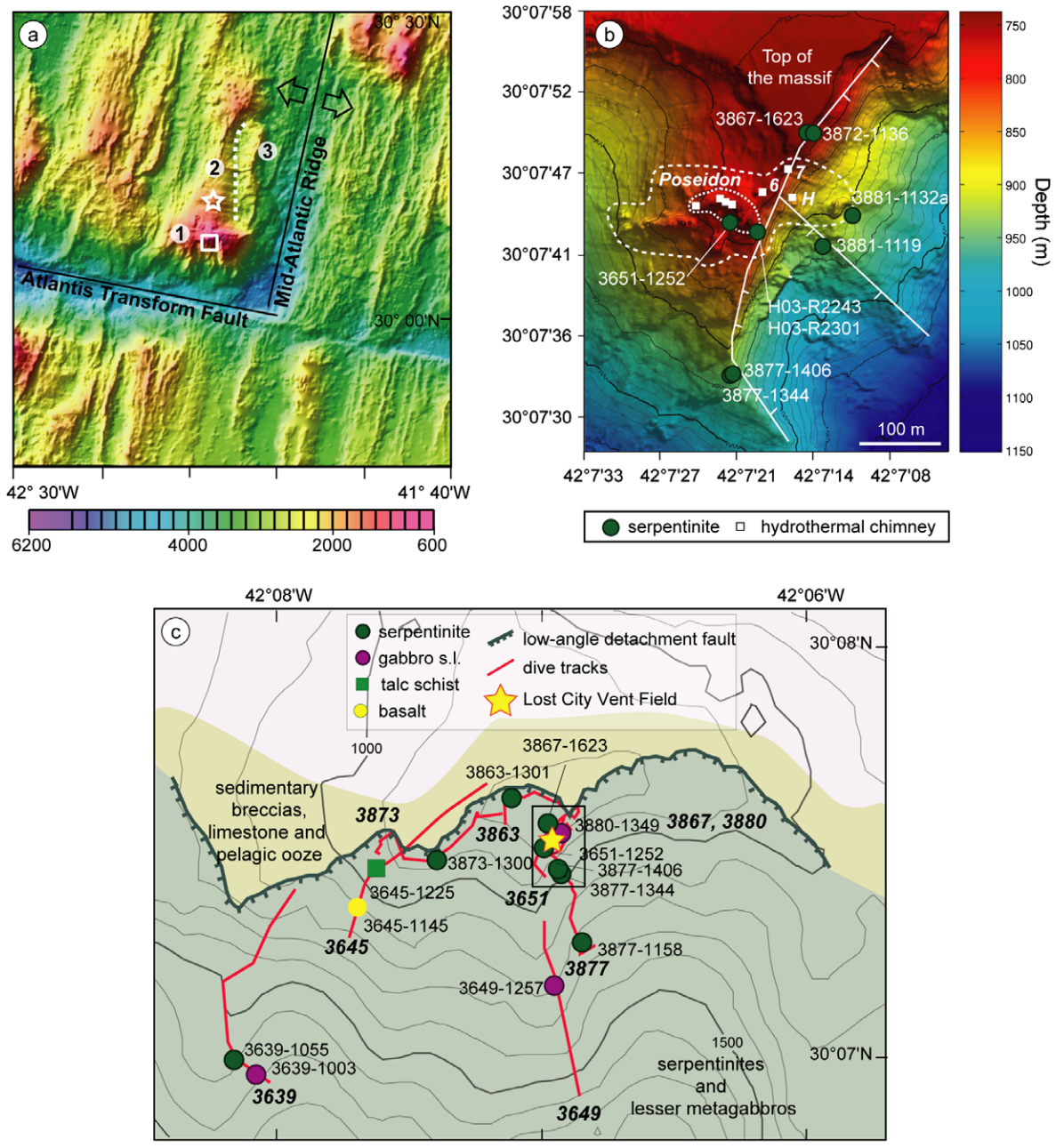

Fig. 1. (a) Location map and morphology of the Atlantis Massif at the inside corner of the intersection between the slow-spreading Mid-Atlantic Ridge and the Atlantis Transform Fault. Based on morphologic and lithologic criteria, this 1.5–2 Myr old massif is divided into three domains: (1) a peridotite-dominated southern ridge; (2) the gabbroic central dome; and (3) the volcanic eastern block. The white box shows the study area along the wall of the southern ridge of the Atlantis Massif and the Lost City Hydrothermal Field, enlarged in (b) and (c). White star: Site U1309 investigated during IODP Expeditions 304 and 305 (Blackman et al., 2006). (b) High resolution map of the Lost City Hydrothermal Field (LCHF) obtained by the autonomous vehicle ABE and gridded at 2 m (Kelley et al., 2005). The external dashed line shows the spatial extent of the active field and major carbonate structures; the internal, finely dashed line indicates the size of the largest, 60 m high, hydrothermal structure Poseidon. The location of the samples investigated in this study are shown relative to the positions of other active structures, identified by field markers 6, H and 7 (shown as solid white squares), as well as the location of normal faults shown by the white hatched lines and discussed by Karson et al. (2006). (c) Simplified geologic map of the top of the southern wall of the Atlantis Massif (Karson et al., 2006) showing the location and lithologies of the samples analyzed in this study and dive tracks from the 2000 and 2003 cruises. Green hatched line: trace of the detachment shear zone (DSZ) at the top of the massif; yellow star: location of the LCHF.

et al., 2006; Brazelton et al., 2006; Karson et al., 2006; Ludwig et al., 2006; Proskurowski et al., 2006; Boschi et al., 2008; Proskurowski et al., 2008). In 2005, the NOAA vessel *R.H. Brown* returned to the LCHF site for high-resolution imagery and sampling of the southern ridge of the massif and the LCHF using the remotely operated vehicle (ROV) *Hercules*. The geochemical study presented here focuses on serpentinized peridotites, metagabbros, one

talc-rich rock and one basalt collected across the southern wall of the AM and the LCHF during the three cruises (Fig. 1b and c). Similar studies of the crustal and upper mantle rocks recovered from IODP Hole 1309D are presented in a companion paper (Delacour et al., this issue). The principal results of the IODP drill core are summarized here to emphasize regional differences.

3.2. Analytical methods

Sulfur isotope analyses and sulfur contents were determined on bulk rock powders and on separate fractions (monosulfides, disulfides and sulfates) using a Carlo Erba Elemental Analyzer (EA) (NCS 2500, CE Instruments) interfaced in continuous flow mode to a GV Instruments OPTIMA mass spectrometer. Preliminary sulfur content and sulfur isotope measurements were made on 52 whole-rock samples (20 serpentinites, 14 talc- and/or amphibole-schists, 17 mafic samples and 1 basalt). Thirty-three of the 52 samples had small or nearly absent sulfur peak, i.e. below the detection limit of ~120 ppm sulfur for bulk rock powder, or showed distinct peak-tailing that hindered accurate measurement of the total sulfur content and isotopic composition. The peak-tailing phenomenon is likely related to the dominance of hydrous phases, such as serpentine and chlorite (Studley et al., 2002). These bulk rock measurements were used to choose the 19 samples containing >~120 ppm total sulfur for extraction of the sulfate and sulfide phases, and for sulfide mineralogy studies.

For extraction of sulfate and sulfide phases, approximately 10–20 g of powdered sample was reacted with HCl and a $CrCl_2$ solution under N_2 atmosphere according to the method of Tuttle et al. (1986). Reaction of the sample powder with HCl dissolved the acid-soluble sulfates and decomposed the monosulfides, liberating H_2S. The H_2S was precipitated as Ag_2S, whereas the liberated acid-soluble sulfates were precipitated as $BaSO_4$. In a second step, the disulfide minerals were reduced by addition of a $CrCl_2$ solution to the sample powder residue. This released H_2S, which was then precipitated and analyzed as Ag_2S. Amounts of collected sulfate-sulfur, monosulfide-sulfur and disulfide-sulfur were determined gravimetrically on a high-precision balance. Sulfate-sulfur contents determined by weight were corrected based on the sulfur content determined by EA. The correction was necessary because during the washing step subsequent to HCl treatment and dissolution, some of the very fine-grained rock powder passed through the filter resulting in an overestimation of the amount of sulfate-sulfur determined gravimetrically. Because carbonates generally contain only a few ppm sulfate (Gellatly and Lyons, 2005), the presence of carbonate in the serpentinites and its dissolution with HCl in the first step of the extraction procedure most likely contributes negligibly to the estimated sulfate-sulfur contents.

For sulfur isotope ratio measurements, approximately 0.5–1 mg of extracted Ag_2S and $BaSO_4$ and approximately 100 mg of bulk rock powder were weighed into tin capsules. Vanadium pentoxide (V_2O_5) was added to the sample in the tin capsule to enhance the combustion. The samples were combusted in the EA and analyzed in continuous flow by isotope ratio mass spectrometry (IRMS). Sulfur isotope values are reported as standard δ-notation relative to the Vienna-Canyon Diablo Troilite (V-CDT) standard. The system was calibrated using the international standards IAEA-S1 ($\delta^{34}S = -0.3‰$), IAEA-S2 ($\delta^{34}S = 22.7‰$), NBS123 ($\delta^{34}S = 17.4‰$) for sulfides, and IAEA-SO5 ($\delta^{34}S = 0.5‰$), IAEA-SO6 ($\delta^{34}S = -34.1‰$) and NBS127 ($\delta^{34}S = 21.1‰$) for sulfates. The detection limit for a reproducible sulfur isotope measurement on the Micromass system was about 28 μg S. Analytical reproducibility of replicate measurements of standards is ±0.3‰ ($n = 319$) and relative precision for the sulfur content is within 3%.

Sulfide phases were identified by reflected light microscopy and their chemical composition was determined with a JEOL JXA-8200 electron microprobe. The operating conditions were 15 kV accelerating potential, 20 nA current, and 1–10 μm beam size. Natural and synthetic sulfide mineral standards were used for calibration. Elemental sulfur from selected serpentinites was extracted with a 1:1 mixture of dichloromethane and methanol and analyzed for sulfur isotope composition with the EA-IRMS.

4. RESULTS

4.1. Mineralogy

4.1.1. Serpentinized peridotites

The southern wall of the AM and areas proximal to LCHF are predominantly composed of depleted spinel harzburgites with medium- to coarse-grained porphyroclastic textures. Primary minerals include olivine, orthopyroxene and chromium spinel that are highly affected by serpentinization (from 70% to 100%) and local metasomatism (Schroeder and John, 2004; Boschi et al., 2006; Karson et al., 2006). Alteration is dominated by the formation of well-developed ribbon to mesh textures of lizardite ± chrysotile and magnetite after olivine. Mg–Al chlorite, talc and amphibole are associated with varying degrees of metasomatic overprinting of earlier serpentine. Orthopyroxene is altered to bastite ± chlorite ± Ca-amphibole ± talc and shows undulose extinction in the less-altered samples. The alteration of orthopyroxene porphyroclasts to Ca-amphibole ± talc ± chlorite postdates an early stage of serpentinization characterized by bastite formation (Boschi, 2006). Bulk rock oxygen isotope compositions of the serpentinites are depleted in ^{18}O ($\delta^{18}O$ +1.7‰ to +5.5‰ V-SMOW) and indicate that alteration was most pervasive at temperatures of ~150–250 °C (Boschi et al., 2008).

Opaque mineralogy in the serpentinites is dominated by magnetite with relics of magmatic Al-spinels rimmed by ferritchromite. The serpentinites are locally cut by several generations of veins filled with serpentine or chlorite ± tremolite ± talc. Calcite veins represent the last vein generation and are related to the formation of the LCHF. Brucite and Fe–Ni alloys, which are common products of olivine serpentinization, were not detected in any of the samples. Brucite is sensitive to silica activity and fO_2, and Fe–Ni alloys are not stable under conditions of high fO_2 or complete serpentinization of the rock (Frost, 1985; Boschi et al., 2008).

Table 2
Description and locations of the samples selected in this study

Sample	Depth (mbsl)	Latitude N	Longitude W	Rock type	Description of the samples	Sulfide phases
3639-1055	1615	30°6.684′	42°8.347′	Serpentinite	Mesh to ribbon serpentine texture; opx relics and few ol relics.	Pentlandite + pyrite
3651-1252	795	30°7.407′	42°6.968′	Serpentinite	Mesh to ribbon serpentine texture; HT deformation of opx	Pyrite
3863-1301	834	30°7.512′	42°7.410′	Serpentinite	Static serpentinization, oxidized and late carb/cc veins	No phase identified
3867-1623	759	30°7.488′	42°7.140′	Serpentinite	Static serpentinization, oxidized and late carb/cc veins	No phase identified
3872-1136	798	30°7.482′	42°7.134′	Serpentinite	Static serpentinization	No phase identified
3873-1300	950	30°7.338′	42°7.776′	Serpentinite	Crystal plastic deformation—ribbon texture	
3877-1158	1115	30°7.026′	42°7.122′	Serpentinite	Local metasomatism	
3877-1344	913	30°7.320′	42°7.206′	Serpentinite	Ribbon serpentine texture	No phase identified
3877-1406	908	30°7.320′	42°7.200′	Serpentinite	Static serpentinization, late carb/cc veins	No phase identified
3881-1119	860	30°7.404′	42°7.128′	Serpentinite	Static serpentinization	Pyrite
3881-1132a	822	30°7.422′	42°7.098′	Serpentinite	Ribbon texture	
H03-R2243	834	30°7.246′	42°7.113′	Serpentinite	Static serpentinization, late carb/cc veins	Pyrite
H03-R2301	820	30°7.246′	42°7.109′	Serpentinite	Minor crystal plastic deformation	Pyrite
3645-1225	955	30°7.354′	42°7.819′	Talc-rich schist		
3645-1145	957	30°7.355′	42°7.826′	Basalt		
3639-1003	1648	30°6.677′	42°8.315′	Gabbro	Plag and px neoblasts, green and brown amphi	Pyrrhotite + pentlandite + chalcopyrite
3646-1138	2393	30°4.904′	42°6.006′	Microgabbro	Doleritic texture	Pyrrhotite + chalcopyrite
3649-1257	1188	30°6.969′	42°7.191′	Gabbro	Plag and px neoblasts, green and brown amphi	Pyrrhotite ± chalcopyrite ± pentlandite ± pyrite
3880-1349	819	30°7.236′	42°7.086′	Oxide gabbro	Plag and px neoblasts, green and brown amphi	Pyrite

Sulfide minerals in the serpentinized peridotites were difficult to detect and characterize due to their small grain size and scarcity (Tables 2 and 3). Secondary pyrite [FeS_2] is dominant, with rare occurrences of pentlandite [$(Fe,Ni)_9S_8$] (Table 2). Pyrite is present as individual grains of 1–10 μm and rarely exceeds 30 μm. It was identified as an interstitial phase between serpentine minerals, and as filling veins (Fig. 2a). In sample 3881-1119, secondary pyrites within a calcite vein show a characteristic framboidal form (Fig. 2b–d) with a typical diameter of 10 μm (Farrand, 1970). Magmatic pentlandite was found only in one serpentinite sample (3639-1055) as 10–15 μm grain mantled by late magnetite (Fig. 2e). Pyrite compositions are similar throughout the serpentinites and show narrow ranges of S and Fe contents from 51.1 to 53.6 wt.% and 45.8 to 46.4 wt.%, respectively, and trace amounts of Cu, Ni and Zn (<0.02 wt.%, <0.51 wt.%, and <0.02 wt.%, respectively). Pentlandite is also characterized by low Cu and Zn concentrations (both ~0.01 wt.%).

Chemical analyses indicate that sulfate is the dominant sulfur phase in the serpentinites (Table 3); however, we were unable to detect crystalline sulfate phases by microscopy, by EDS mapping and punctual analyses, by Raman spectroscopy, or by X-ray diffraction. Alt and Shanks (1998, 2003) reported similar results, and were unable to identify the sulfate phases in serpentinites with high sulfate contents recovered at Iberian Margin, Hess Deep and MARK area. Experiments by Seyfried and Dibble (1980) and Janecky and Seyfried (1986) indicate that Mg-hydroxy-sulfate should be produced during reactions of peridotite with seawater at 300 °C. An explanation for this discrepancy may be that sulfate is present as an adsorbed phase in the serpentine structure or on the surface of the magnetite grain. Experimental studies report the affinity of sulfate to be adsorbed in phyllosilicate-like mineral (e.g., kaolinite) or in amorphous iron oxide (Inskeep, 1989; Geeldhoed et al., 1997).

4.1.2. Gabbroic rocks

Gabbroic rocks recovered from the southern wall of the AM are dominated by medium- to coarse-grained gabbros with less common gabbronorites, olivine-bearing gabbros, oxide gabbros, pyroxenites, microgabbros, and diabase dikes. Primary minerals include clinopyroxene and plagioclase, with minor orthopyroxene, olivine and oxide phases. Mylonitic gabbros show crystal-plastic deformation under granulite to amphibolite facies metamorphic conditions (Schroeder and John, 2004; Boschi et al., 2006; Karson et al., 2006). Pyroxenes are commonly converted to pyroxene neoblasts, indicative of granulite/amphibolite facies recrystallization and are altered to brown and green amphibole (tremolite ± actinolite) and chlorite (Schroeder and John, 2004). Magmatic plagioclase is altered to secondary plagioclase and is locally replaced by prehnite ± zeolite, indicating lower temperature alteration (~150–250 °C). The oxide gabbros contain >2% modal primary Fe–Ti

Table 3
Sulfur contents and sulfur isotope compositions of bulk rock, and extracted sulfide and sulfate of serpentinites, talc-schist, basalt, and gabbros collected at the southern wall of the Atlantis Massif

Sample	Type	Depth (mbsl)	Mono-sulfide-sulfur content (ppm)	Disulfide-sulfur content (ppm)	Sulfate-sulfur content (ppm)	Elemental sulfur content (ppm)	Total sulfur content (ppm)	SO_4/S_{total}	$\delta^{34}S$ mono-sulfide (‰)	$\delta^{34}S$ disulfide (‰)	$\delta^{34}S$ sulfate (‰)	$\delta^{34}S$ S^0 (‰)	$\delta^{34}S$ bulk rock (‰)[a]	$\delta^{34}S$ bulk rock EA (‰)[b]
3639-1055	Serpentinite	1615	0	39	705	n.d.	744	0.95	n.d.	−22.9	20.2	n.d.	17.9	16.3
3651-1252	Serpentinite	795	0	11	566	6.0	577	0.98	n.d.	10.7	6.1	−5.7	6.2	9.0
3863-1301	Serpentinite	834	0	14	332	n.d.	346	0.96	n.d.	14.9	21.1	n.d.	20.9	19.0
3867-1623	Serpentinite	759	0	13	272	n.d.	285	0.95	n.d.	13.9	22.0	n.d.	21.6	20.2
3872-1136	Serpentinite	798	0	15	108	n.d.	123	0.88	n.d.		21.4	n.d.		18.0
3873-1300	Serpentinite	950	0	15	132	n.d.	147	0.90	n.d.	7.9	20.5	n.d.	19.2	18.2
3877-1158	Serpentinite	1115	5	15	214	n.d.	234	0.91	n.d.	8.8	21.7	n.d.	20.4	19.7
3877-1344	Serpentinite	913	3	14	244	n.d.	261	0.93	n.d.	13.4	20.5	n.d.	19.9	18.7
3877-1406	Serpentinite	908	5	27	170	n.d.	202	0.84	n.d.	8.2	20.8	n.d.	18.6	18.3
3881-1119	Serpentinite	860	144	1718	466	167	2328	0.20	−6.2	−6.0	−8.3	−5.3	−6.5	−8.4
3881-1132a	Serpentinite	822	0	13	231	n.d.	244	0.95	n.d.	11.0	19.8	n.d.	19.3	12.5
H03-R2243	Serpentinite	834	172	588	333	n.d.	1093	0.30	27.1	19.4	19.7	n.d.	20.7	n.d.
H03-R2301	Serpentinite	820	102	4563	732	n.d.	5397	0.14	20.0	16.3	15.9	n.d.	16.3	n.d.
3645-1225	Talc-schist	955	0	10	15	n.d.	25	0.60	n.d.	7.7	20.3	n.d.	15.3	19.3
3639-1003	Gabbro	1648	371	238	Trace	n.d.	612	0.00	−2.3	−1.7	n.d.	n.d.	−2.1	n.d.
3646-1138	Gabbro	2393	406	984	Trace	n.d.	1391	0.00	−0.3	−1.7	n.d.	n.d.	−1.3	n.d.
3649-1257	Gabbro	1188	68	165	3	n.d.	236	0.01	0.6	−1.7	3.6	n.d.	−1.0	0.2
3880-1349	Gabbro	819	311	4084	1627	n.d.	6022	0.27	17.6	5.5	11.0	n.d.	7.6	8.3
3645-1145	Basalt	957	22	205	15	n.d.	242	0.06	−2.5	−1.5	16.9	n.d.	−0.5	n.d.

[a] $\delta^{34}S$ values of the bulk rock obtained by mass balance calculations.
[b] $\delta^{34}S$ values of the bulk rock measured with the EA-IRMS.

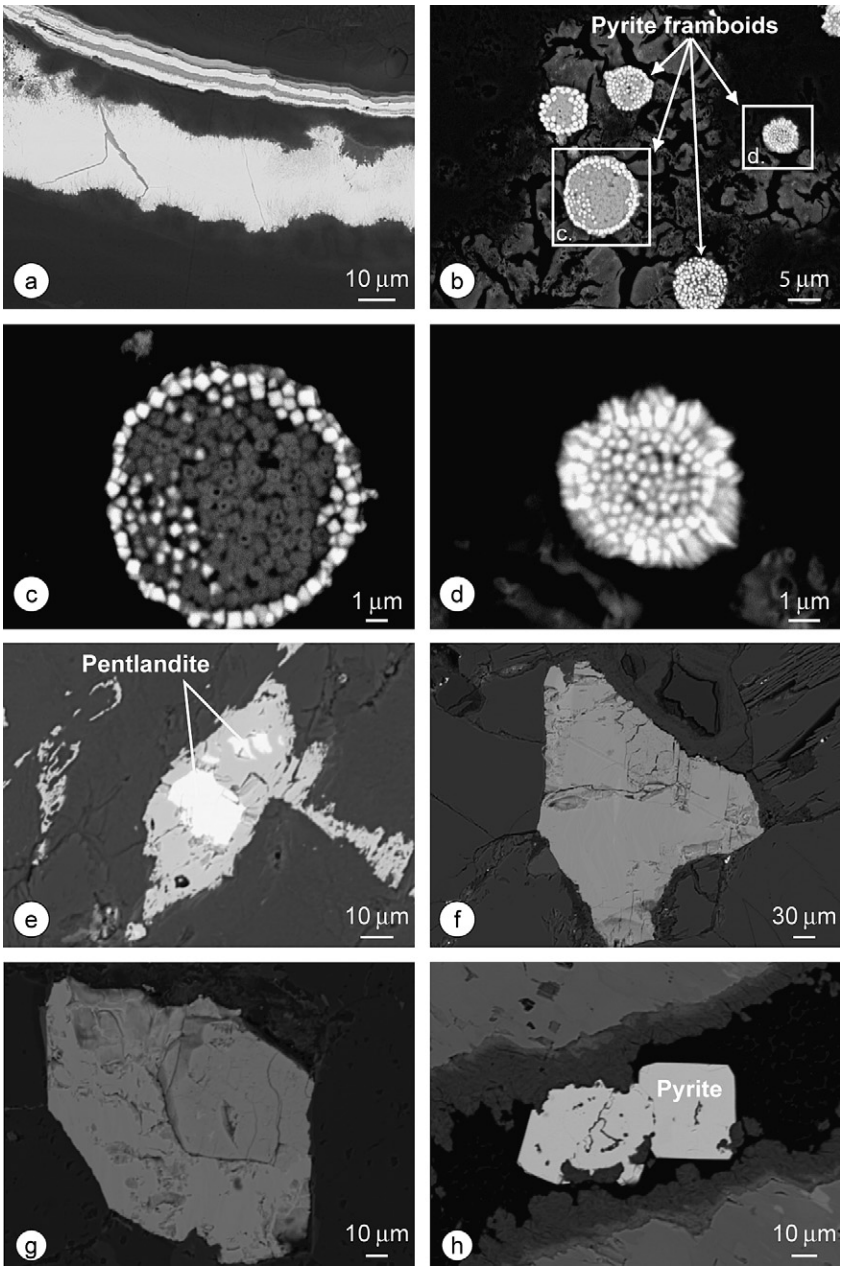

Fig. 2. Backscattered electron (BSE) microprobe images of sulfide minerals. (a) Pyrite veins cutting the serpentine mesh texture of serpentinite sample H03-R2301; (b) aggregate of pyrite framboids within a calcite vein in serpentinite sample 3881-1119. The white boxes (c) and (d) correspond to the close-up images in (c) and (d), which show BSE imaging of a pyrite framboid. The inner structure of the framboid is visible with the microcrystal grains of pyrite of about 0.5–1 μm in size. (e) Pentlandite enclosed in magnetite in serpentinite sample 3639-1055; (f) pyrrhotite grain in gabbro 3639-1003; (g) chalcopyrite grain in gabbro 3639-1003; and (h) pyrite grain in a vein in oxide-gabbro 3880-1349.

oxides, and are characterized by total Fe_2O_3 content >25 wt.%. Opaque phases are mainly magnetite and ilmenite.

The sulfide minerals in the gabbros consist of an assemblage of pyrrhotite ± chalcopyrite ± pentlandite ± pyrite (Table 2). Primary pyrrhotite [$Fe_{1-x}S$, $x = 0 - 0.2$] is most common, occurring as individual grains 30–50 μm across (Fig. 2f) or as interstitial phases. Magmatic chalcopyrite [$CuFeS_2$] forms grains 5–70 μm in size (Fig. 2g). Primary pentlandite is less common and occurs as grains 20–100 μm across that are associated with pyroxene minerals. Two samples, the oxide gabbro 3880-1349 and sample 3649-1257, contain secondary pyrite as disseminated grains, 10–100 μm in size, in the matrix and in pyroxene grains and veins (Fig. 2h).

The chemical compositions of the sulfides in the serpentinized peridotites and the gabbros are shown in a ternary diagram S–Fe-(Cu, Ni) in Fig. 3. Cu and Ni cluster at the same apex, and thus pentlandite and chalcopyrite plot in the same area. In sample 3649-1257, pyrite grains are either

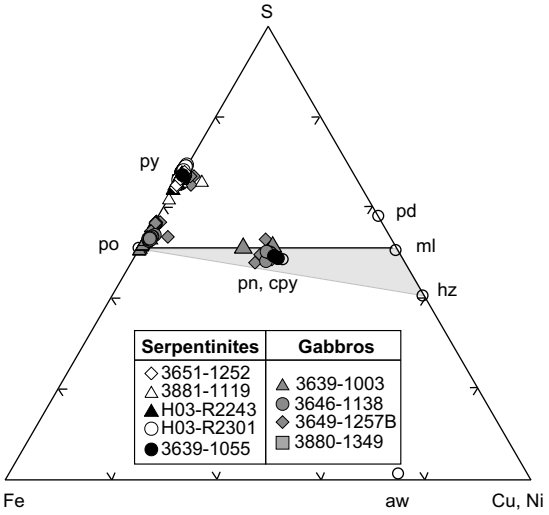

Fig. 3. Ternary plot Fe–S–(Cu,Ni) showing the chemical composition (based on atomic proportions) of the sulfide minerals analyzed by electron microprobe. The sulfur assemblages of the serpentinites of the AM-LCHF are dominated by pyrite with rare pentlandite. The gabbros show an assemblage pyrrhotite ± chalcopyrite ± pentlandite ± pyrite. These high-sulfur assemblages indicate more oxidizing conditions than sulfur assemblages normally formed during reducing conditions of serpentinization at low water–rock ratios. The gray shaded area represents the Ni-rich low-sulfur sulfide assemblages of the olivine-rich rocks at the central dome (data are from Delacour et al., this issue). Mineral abbreviations: py: pyrite; po: pyrrhotite; pd: polydymite; pn: pentlandite; cpy: chalcopyrite; ml: millerite; hz: heazlewoodite; aw: awaruite.

enriched in Ni and/or Cu, with concentrations up to 1.4 wt.% and to 2.7 wt.%, respectively. Pyrrhotite shows a small range of S and Fe contents (~37.7 wt.% and 57.4% to 60.8 wt.%, respectively), low contents of Cu and Zn (<0.02 wt.%) and moderately high amounts of Ni (0.18–1.1 wt.%). Chalcopyrite contains minor Ni and Zn (0.02–0.2 wt.%) and pentlandite has low Cu and Zn contents (0.02–0.2 wt.%).

4.2. Sulfur content and sulfur isotope compositions

Depleted mantle peridotites, resulting from 15–20% melting, generally contain ~60–120 ppm total sulfur (Alt and Shanks, 2003) and have $\delta^{34}S$ values of $+0.1 \pm 0.5‰$ (Sakai et al., 1984; Alt et al., 1989; Shanks et al., 1995; Shanks, 2003). In comparison, the serpentinized peridotites at the southern wall are characterized by ^{34}S-enriched bulk rock sulfur isotope compositions, variable total sulfur contents, and a dominance of sulfate-sulfur over sulfide-sulfur contents (Table 3). A large number of samples analyzed initially yielded distinctly low total sulfur contents (<~120 ppm), in the range of magmatic sulfur contents for depleted peridotites. However, chemical extraction of the serpentinites indicates that sulfur is mainly present as sulfate, implying low sulfide contents and alteration of the southern wall serpentinites under conditions that promoted removal of sulfide-sulfur. The remaining serpentinites show total sulfur contents between 123 and 5397 ppm and bulk rock $\delta^{34}S$ values ranging from −6.5‰ to +21.6‰ (Table 3). Most samples fall within a narrower range from +16.3‰ to +21.6 ‰, which reflects incorporation of seawater sulfate (Fig. 4a). The one talc-rich sample has a distinctly low total sulfur content of 25 ppm and is slightly depleted in ^{34}S (bulk $\delta^{34}S$ value of +15.3‰) compared to the serpentinites. Bulk rock $\delta^{34}S$ values of the gabbros range from −2.1‰ to +7.6‰ and total sulfur contents range from 236 to 6022 ppm. The basalt sample lies at the lower end of this range with 242 ppm total sulfur and a mantle-like bulk $\delta^{34}S$ value of −0.5‰.

Sulfur in the serpentinites occurs mainly as sulfate, with a SO_4/S_{total} ratio ranging from 0.14 to 0.98, in contrast to ratios of <0.27 in the gabbros, and 0.06 and 0.60 for the basalt and talc-rich rock, respectively (Table 3 and Fig. 4a). The concentration of sulfide-sulfur in the serpentinites is generally less than 100 ppm, but varies from 760 to 4665 ppm in three samples and is distinctly low in the talc schist sample (10 ppm). The mafic rocks have sulfide-sulfur contents from 227 to 4395 ppm. Sulfate-sulfur contents range from 108 to 732 ppm in the serpentinized peridotites, from trace to 1627 ppm in the gabbros, and are 15 ppm in both the basalt and talc-rich rock. Three serpentinite samples (3881-1119, H03-R2243 and H03-R2301) are distinct from the majority of the samples and are characterized by low SO_4/S_{total} ratios (0.20, 0.30 and 0.14, respectively) and high sulfate-sulfur contents, which indicate that these samples have gained both sulfate-sulfur and sulfide-sulfur (Table 3, Fig. 5).

The S-isotope compositions of the disulfides in the serpentinites are also variable, with $\delta^{34}S$ ranging from depleted compositions of −22.9‰ to near seawater values of +19.4‰. In contrast, the disulfides in the mafic rocks show a narrower range of $\delta^{34}S$ values of −1.5‰ to +5.5‰. The monosulfides range from −6.2‰ to +27.1‰ in the serpentinites and from −2.3‰ to +17.6‰ in the gabbros (Fig. 4b and c). Sulfate-sulfur in the serpentinites shows more variable isotopic compositions than the gabbros, with $\delta^{34}S_{sulfate}$ values of −8.3‰ to +22.0‰ and +3.6‰ to +11.0‰, respectively (Fig. 4b).

Organic solvent extraction of samples 3881-1119 and 3651-1252 yielded 167 and 6 ppm elemental sulfur, respectively (Table 3), whereas the amounts of elemental sulfur in the other extracted sample (H03-R2301) were too low to be quantified. The $\delta^{34}S$ values of the elemental sulfur fractions were −5.3‰ and −5.7‰ for samples 3881-1119 and 3651-1252 (Table 3), respectively. The wide variations in sulfur content and isotopic compositions of the basement rocks at the southern wall point to multiple sources of sulfur and, as discussed below, suggest that a number of processes have been active during the alteration history of the Atlantis Massif.

5. DISCUSSION

Oxide and sulfide mineral assemblages and sulfur geochemistry of the serpentinites reflect the net effect of variations in temperature, fluid–rock interaction, fS_2 and fO_2 conditions, and biological activity during long-lived serpentinization and alteration of the AM. As in basaltic systems, seafloor peridotite-hosted hydrothermal systems have two main sources of sulfur: seawater sulfate ($\delta^{34}S = +21‰$)

and mantle sulfides ($\delta^{34}S = +0.1 \pm 0.5‰$). The effects of the main abiotic and biotic processes on sulfur geochemistry are summarized in Fig. 6.

Oxygen, hydrogen, boron, and strontium isotope data indicate that serpentinization at the southern wall of the AM was a seawater-dominated process at integrated temperatures of 150–250 °C (Früh-Green et al., 2002; Delacour et al., 2005; Boschi et al., 2008). Somewhat lower temperatures of 110–150 °C have been calculated for the present-day thermal regime of serpentinization from CH_4-H_2 isotope fractionations in the vent fluids (Proskurowski et al., 2006). These temperature estimates are in agreement with the theoretical model of Allen and Seyfried (2004), which predicts that serpentinization at LCHF occurs at temperature of 200 °C ± 50 °C. Results of mineralogical and geochemical studies (e.g., lack of clays, no Mg loss, no high Rb contents) indicate a lack of significant seafloor weathering (Boschi, 2006; Boschi et al., 2008). Modeling of Sr and Nd isotope compositions of the southern AM serpentinites indicate that water–rock ratios range from ~20 up to 10^6 with progressive serpentinization (Delacour et al., 2005; Delacour et al., 2008a). The serpentinite samples collected at the southern wall are considered to represent the "outer skin" of the Lost City hydrothermal system and therefore are the end-products of long-lived seawater-peridotite interaction at moderate temperatures (Boschi et al., 2008). This long-lived history of alteration most likely overprints any products of early stages of serpentinization, such as those observed in other studies (Frost, 1985; Alt and Shanks, 1998, 2003; Palandri and Reed, 2004). In the following, we first constrain in more detail the oxygen and sulfur fugacity of the system and discuss the main processes responsible for the removal and addition of different sulfur species under high fluid–rock ratios.

5.1. Chemical and mineralogical constraints on oxygen and sulfur fugacity

Fertile mantle peridotites contain ~250–300 ppm total sulfur, present as sulfide, and these concentrations decrease with partial melting (Ringwood, 1966; Sakai et al., 1984; Lorand, 1991; Hartman and Wedepohl, 1993). The peridotites at the AM have spinel compositions typical of those of depleted abyssal harzburgites in the Atlantic and indicate a

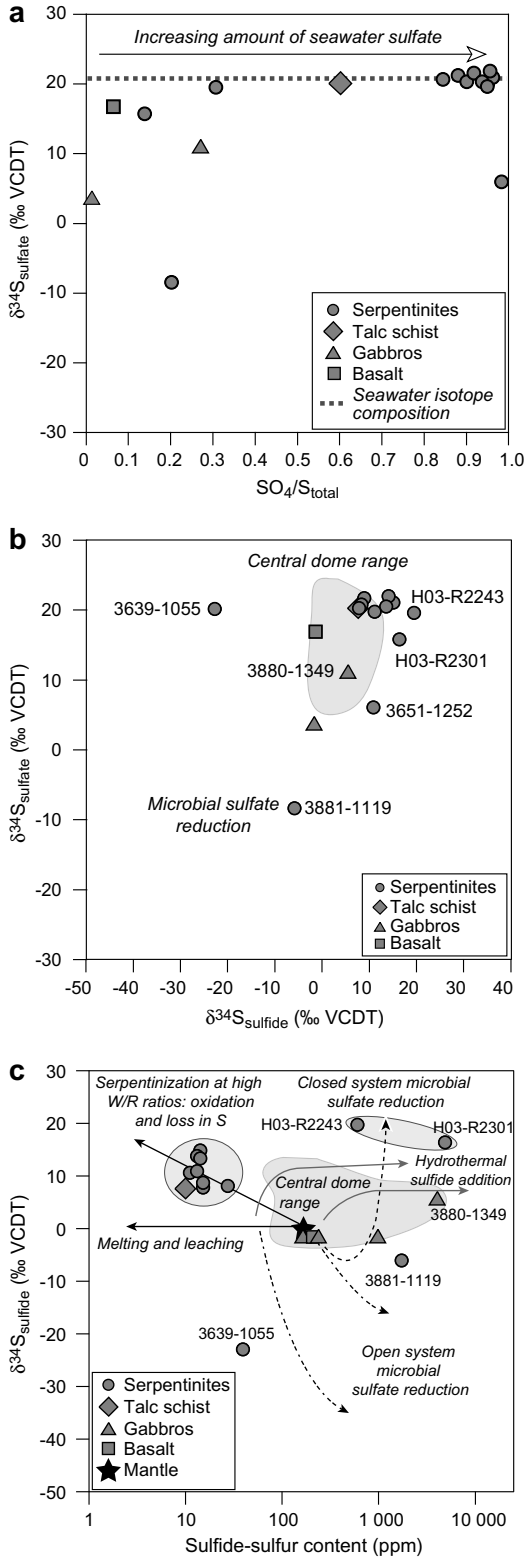

Fig. 4. Sulfur contents and sulfur isotope compositions of the serpentinites, talc-schist, basalt and gabbros from the southern wall of the Atlantis Massif (note that in these diagrams the sulfide content represents solely the disulfide content of the samples). (a) $\delta^{34}S_{sulfate}$ against SO_4/S_{total} ratios show that most of the serpentinites have high $\delta^{34}S_{sulfate}$ values and high SO_4/S_{total} ratios indicating incorporation of seawater sulfate. (b) $\delta^{34}S_{sulfate}$ plotted against the $\delta^{34}S_{sulfide}$, showing the variable $\delta^{34}S$ values of the serpentinites and gabbros. The range of compositions of the olivine-rich rocks at the central dome is shown as shaded area for comparison (data from Delacour et al., this issue). (c) $\delta^{34}S_{sulfide}$ plotted against sulfide-sulfur content indicating that most of the serpentinites are grouped with high $\delta^{34}S_{sulfide}$ values toward seawater sulfur isotope composition and low sulfide-sulfur contents. Two samples, H03-R2243 and H03-R2301, show high $\delta^{34}S_{sulfide}$ values and high sulfide-sulfur contents (see text for discussion). Processes influencing the sulfur isotope compositions and sulfur contents of sulfides in rock samples have been added to show variations that can occur in these systems. Arrows and curves are from Alt et al. (2007).

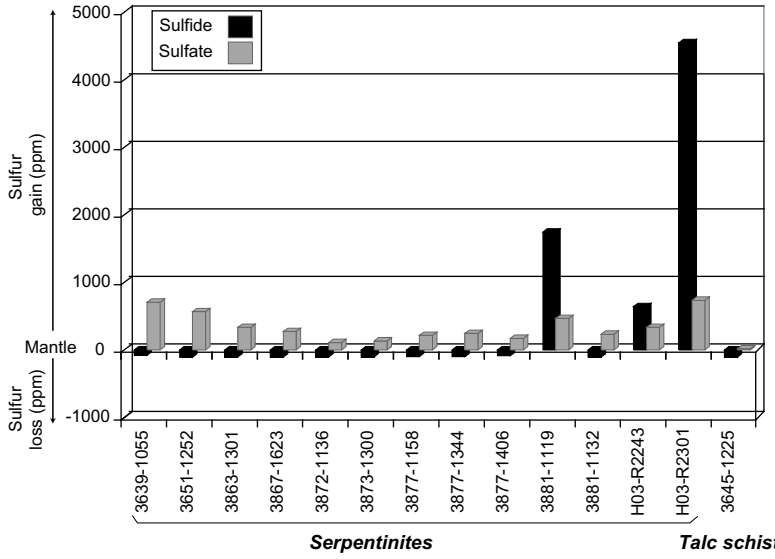

Fig. 5. Histogram showing the gain and/or loss of sulfide and sulfate contents for the serpentinized peridotites and talc-schist of the southern wall of the AM, compared to a sulfur content of depleted mantle of 120 ppm (corresponding to 8–18% of melting; Boschi, 2006). The serpentinites and the talc-schist show a loss of sulfides and variable gain of sulfates, except three samples (3881-1119, H03-R2243 and H03-R2301) that show both enrichment in sulfide and sulfate contents.

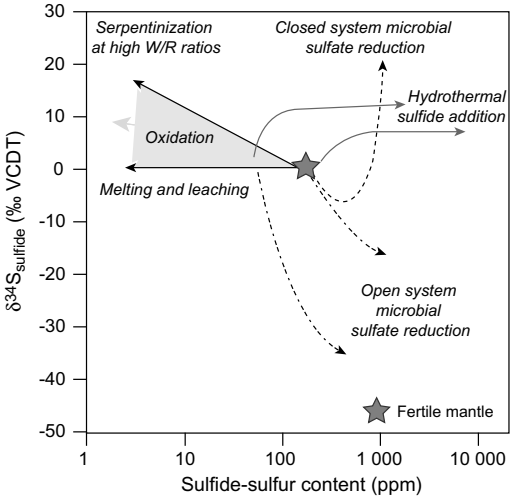

Fig. 6. Schematic diagram showing the main processes affecting sulfur speciation and how fluid-rock interaction, changes in fS_2 and fO_2, and biological activity affect the sulfur contents and sulfur isotope compositions of sulfides during serpentinization and hydrothermal alteration. Melting or leaching of sulfides leads to a decrease in sulfide-sulfur contents with no isotope fractionation. Oxidation of sulfides leads to a decrease in sulfide-sulfur contents with kinetic isotope fractionation producing low $\delta^{34}S_{sulfate}$ values and high $\delta^{34}S_{sulfide}$ values. Hydrothermal sulfide addition, via leaching of igneous sulfides during high-temperature alteration of gabbroic rocks, inorganic sulfate reduction of seawater sulfates, and precipitation of sulfides in serpentinites during low-temperature serpentinization, leads to an increase in sulfide-sulfur contents with enrichment in ^{34}S. Microbial sulfate reduction is favored during low-temperature serpentinization and produces an increase in sulfide-sulfur contents with low $\delta^{34}S_{sulfide}$ values for an open-system and high $\delta^{34}S_{sulfide}$ values for closed system. Curves are from Alt et al. (2007).

variable but relatively high degree of melting ranging from ~8% to 18% (Boschi, 2006). Assuming similar degrees of melting, Alt and Shanks (2003) estimated sulfide-sulfur contents of 60–120 ppm in the depleted residual mantle. Compared to these values, the AM serpentinites show a loss of primary sulfide-sulfur and variable gains in sulfate-sulfur (Fig. 5). A general loss of sulfide-sulfur is further indicated by the lack of detectable monosulfides and low disulfide-sulfur contents in most of the serpentinites (Table 3). Moreover, a net sulfide loss in most of the rocks is consistent with the fact that 75% of the preliminarily bulk rock sulfur analyses yielded total sulfur contents less than ~120 ppm, whereby all of the extracted serpentinites have high SO_4/S_{total} ratios (Table 3) that reflect low sulfide contents. On the other hand, approximately 50% of the extracted samples shown in Table 3 have total sulfur concentrations greater than mantle values (reaching up to ~0.5 wt%), indicating local incorporation of a significant amount of sulfur during serpentinization. With the exception of three samples, 85–95% of the total sulfur in the serpentinites from the southern AM is in the form of sulfate (Table 3). We conclude that the low sulfide contents are the result of mobilization/dissolution and subsequent oxidation of igneous sulfides by circulating seawater. Solubility and mobilization of sulfides are enhanced by higher fO_2 and the presence of sulfate-rich fluids, such as seawater (Frost, 1985).

Assuming the conditions of 300 °C and 2 kbars used by Frost (1985) to construct the diagram in Fig. 7, the opaque mineral assemblages in the serpentinized peridotites and gabbros of the southern wall indicate a fO_2 of 10^{-32} and a fS_2 of 10^{-1}. These are higher than those normally believed to prevail during serpentinization at low water–rock ratios (Eckstrand, 1975; Frost, 1985; Früh-Green et al., 2004). As discussed by Alt and Shanks (1998), the topology of the

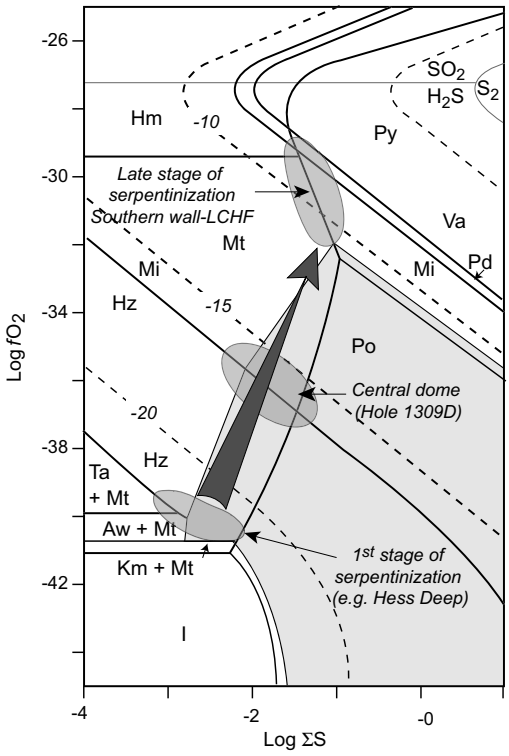

Fig. 7. Log fO_2-log ΣS (where ΣS represents the sum of the activities of the sulfur species) diagram showing the stabilities of oxide and sulfide minerals during serpentinization (from Alt and Shanks, 1998, modified after Frost, 1985). Heavy solid lines show mineral reaction boundaries at 300 °C and 2 kbars, calculated from thermodynamic data and inferred from petrologic data. Light gray solid lines represent the boundaries between dominant sulfur species, and dashed lines show contours of log fS_2 in the fluid. Shaded area is the stability field of pentlandite. The arrow shows the evolution from highly reducing conditions (pyrrhotite + pentlandite + Fe–Ni alloys) that commonly prevail during early stages of serpentinization at low water–rock ratios (such as at Hess Deep, Alt and Shanks, 1998), to an assemblage of pentlandite + millerite + heazlewoodite, which characterizes the reducing conditions at the central dome, and finally to an assemblage of magnetite + pyrite dominant (Delacour et al., this issue) during oxidizing conditions at high water–rock ratios as documented at the southern AM-LCHF. For conditions of 300 °C and 2 kbars, this assemblage corresponds to fO_2 of 10^{-32} and $f\Sigma S$ of 10^{-1}. Mineral abbreviations: Py: pyrite; Po: pyrrhotite; Pd: polydymite; Mt: magnetite; Mi: millerite; Hz: heazlewoodite; Aw: awaruite; Hm: hematite; Va: valleriite; Ta: taenite; Km: kamacite; I: iron.

fO_2-$f\Sigma S$ diagram (Fig. 7) is similar for lower temperatures, but the absolute values for fO_2 and fS_2 will be different. In this study, thermodynamic calculations were carried out for lower temperature conditions (150–200 °C) based on the equilibrium magnetite–pyrrhotite–pyrite and using the thermodynamic data of Frost (1985). These calculations yielded fO_2 values of $\sim 10^{-43}$ and fS_2 of $\sim 10^{-3.5}$ at 200 °C and fO_2 of $\sim 10^{-50}$ and fS_2 of $\sim 10^{-4}$ at 150 °C; these values are similar to those calculated by Eckstrand (1975) for a temperature of 127 °C.

The high sulfur-bearing assemblages (Figs. 3 and 7) of the serpentinites and gabbros are similar to calculated sulfide mineral assemblages based on geochemical modeling of serpentinization at 300 °C and at high water–rock ratios (Alt and Shanks, 2003; Palandri and Reed, 2004) and indicate slightly more oxidizing conditions at the southern wall of the AM than at Hess Deep (Alt and Shanks, 1998) and at IODP Site U1309 at the central dome (Delacour et al., this issue). Although temperatures of serpentinization are likely different, the oxygen and sulfur fugacities prevailing at Lost City are similar to the conditions inferred for late stages of alteration in serpentinites of MARK, Iberian Margin and at Hole 1268A (MAR 15° 45′N) (Alt and Shanks, 1998, 2003; Bach et al., 2004). The studies of Frost (1985) and Palandri and Reed (2004) predict the occurrences of hematite and carbonate under relatively oxidizing conditions. Some hematite was observed petrographically and with electron microprobe in our samples.

5.2. Sulfate uptake and sulfide oxidation during progressive serpentinization and seawater influx

In general, the serpentinites have bulk rock and sulfate-sulfur $\delta^{34}S$ values indicating uptake of seawater sulfate (Fig. 4a and b). This is consistent with the work of Alt and Shanks (1998) who documented similar or greater relative gains in sulfate-sulfur from modern oceanic serpentinites at other areas and conclude that oceanic serpentinites may represent a sink for seawater sulfate (e.g., Hess Deep).

The sulfur isotope compositions of the sulfide phases, on the other hand, are either highly enriched or depleted in ^{34}S compared to unaltered mantle compositions with sulfide concentrations either higher or lower than the precursor mantle rock (Figs. 4c and 5). This requires multiple processes to explain the scatter. If the increase in $\delta^{34}S$ is associated with an increase in sulfide concentrations, reduction of seawater sulfate under closed-system conditions or hydrothermal sulfide addition via sulfide leaching from gabbroic rocks during high-temperature hydrothermal alteration are possible processes (Fig. 6). In contrast, an increase in $\delta^{34}S_{sulfide}$ associated with a decrease in sulfide concentration requires removal of magmatic sulfides by dissolution and subsequent oxidation by circulating seawater. We thus postulate that the observed low concentrations in sulfides that are enriched in ^{34}S could be related to processes involving dissolution, partial oxidation and re-precipitation (see below).

In the AM serpentinites, secondary pyrite is the predominant sulfide phase with only rare pentlandite. Conversion of pyrrhotite to pyrite may occur during loss of iron, sulfidization by H_2S, oxidation by O_2, or oxidation/sulfidization by SO_4^{2-} (Gitlin, 1985; Schoonen and Barnes, 1991; Shanks et al., 1995; Shanks, 2003). Based on reaction stoichiometry, Shanks and Seyfried (1987) estimated that $\delta^{34}S$ values of pyrite produced by oxidation/conversion of pyrrhotite with SO_4^{2-} as oxidizing agent would be about 3.0‰. Pyrite may also precipitate from Fe- and S-rich hydrothermal solution by leaching and remobilization of primary igneous sulfides at high temperature (Alt and Shanks, 2003), which is associated with a small sulfur isotope fractionation (Ohmoto and Rye, 1979). As these

processes produce small changes in sulfur isotope composition, they cannot properly explain the high $\delta^{34}S$ values observed for the sulfides in the AM serpentinites.

Although most studies on sulfide oxidation in the literature only report small isotope effects, in which the product sulfate is isotopically heavier than the sulfide (e.g., Ohmoto and Rye, 1979; Pisapia et al., 2007; Brunner et al., 2008), two experimental studies report large kinetic isotope fractionations during sulfide oxidation, where the residual sulfides are enriched in ^{34}S (Fry et al., 1988; Grinenko and Mineyev, 1992). Kinetic isotope fractionation may occur during sulfide oxidation when aqueous sulfide, intermediate sulfoxyanions, and/or biological activity are involved in the reaction (Toran and Harris, 1989). The most important difference between the studies of Fry et al. (1988) and Grinenko and Mineyev (1992) and all other studies is that the experiments were conducted at pH 8–11 rather than at pH 1–4, typical of acid mine tailings. The speciation of sulfur oxyanions in solution is strongly pH dependent. For example, the experimental study of sulfide oxidation by Goldhaber (1983) showed that at low pH, sulfate and tetrathionate are the main oxyanions formed during pyrite oxidation, whereas increases in pH were accompanied by an increase in the concentration of thiosulfate and sulfite. Fry et al. (1988) conducted sulfide oxidation experiments at pH 8.2–11 and showed kinetic fractionations in the range of $-4.1‰$ to $-7.5‰$. These authors attributed the larger kinetic isotope fractionations in their experiments to a cross-reaction between sulfite and sulfide. These fractionations would only be observable at high pH where higher concentrations of sulfite are present (Goldhaber, 1983). We thus conclude that because the fluids produced during serpentinization have high pH, larger kinetic isotope fractionations may be produced during sulfide oxidation in ultramafic systems. Support for this interpretation comes from the work of Grinenko and Mineyev (1992) who conducted leaching experiments on gabbroic rocks at 60–90 °C. While sulfide dissolution did not significantly enrich the residual solid sulfide in ^{34}S, their experiments produced a ^{34}S-enriched secondary sulfide phase, which was derived from partial oxidation of aqueous sulfides to intermediate oxidized sulfur compounds (sulfite, thiosulfate and polythionate). The formation of ^{34}S-enriched sulfides was observed only in the presence of magnetite, which buffered the oxygen fugacity to relatively low values, but not in experiments with gabbros not containing magnetite, where the oxygen fugacity was higher.

Summarizing, high fluid fluxes at Lost City resulted in an increase in oxygen fugacity and nearly complete dissolution of the magmatic sulfides. Transport and re-precipitation of pyrite after partial oxidation of dissolved H_2S led to low sulfide contents with high $\delta^{34}S$ values characteristic of many of the serpentinites at the southern wall (Fig. 4b and c and Table 3). The observed fractionations are consistent with the high pH of ultramafic-derived fluids and the calculated oxygen fugacities (Fig. 7).

Because all of the 19 extracted serpentinites have sulfate-sulfur contents >100 ppm, we can conclude that the other 33 samples, which contained total bulk sulfur contents <∼120 ppm and which were not further extracted, must contain less than 20 ppm of sulfide-sulfur. Therefore, we propose that sulfide oxidation is a dominant process during serpentinization at Lost City. Because the experimental works of Fry et al. (1988) and Grinenko and Mineyev (1992) show kinetic fractionation at temperatures lower that 100 °C and isotope effects are expected to decrease with increasing temperature, we suggest that sulfide oxidation is a probably late-stage process occurring at the lower range of temperatures estimated for the Lost City hydrothermal system (110–250 °C; Proskurowski et al., 2006; Boschi et al., 2008).

5.3. Biogenic processes

Five serpentinite samples, 3881-1119, 3651-1252, 3639-1055, H03-R2243 and H03-R2301 plot outside of the compositions defined by the majority of the AM-LCHF serpentinites (Fig. 4b and c) and have isotopic signatures indicative of microbial sulfate reduction occurring under open- or closed-system conditions in the basement. Microbial sulfate reduction takes place at low temperature (up to 110 °C; Stetter, 1996) and is typically associated with a large sulfur isotope fractionation of 20–70‰ (Goldhaber and Kaplan, 1980; Brunner and Bernasconi, 2005). In contrast, inorganic sulfate reduction can only take place at temperatures above ∼100–150 °C (Andrews, 1979; Ohmoto and Lasaga, 1982; Goldhaber and Orr, 1995; Machel et al., 1995) and occurs through conversion of organic matter (thermochemical sulfate reduction), oxidation of ferrous iron, or by conversion of igneous pyrrhotite to secondary pyrite. Inorganic sulfate reduction is dominated by kinetic isotopic effects that produce variable sulfur isotope fractionations depending on the temperature conditions and the reaction progress (Mottl et al., 1979; Shanks and Seyfried, 1987; Machel et al., 1995; Ohmoto and Goldhaber, 1997). Temperatures of 110–150 °C estimated for serpentinization beneath the largest carbonate structure Poseidon (Proskurowski et al., 2006) are within the range of temperature conditions favorable for inorganic sulfate reduction, and are at the upper limit for microbial sulfate reduction. However, under the conditions of high-integrated fluid fluxes, slightly oxidizing conditions, and high pH prevailing at the southern wall of the AM, inorganic sulfate reduction would be kinetically inhibited.

Samples 3881-1119 and 3639-1055 exhibit moderately to highly negative $\delta^{34}S_{sulfide}$ values of $-6.0‰$ and $-22.9‰$, respectively. The $\delta^{34}S_{sulfide}$ values of these two samples are consistent with microbial sulfate reduction under relatively open conditions where continuous replenishment of sulfate can lead to the production of sulfide with $\delta^{34}S$ in the range $-40‰$ to $-20‰$ (Goldhaber and Kaplan, 1980). Microbial sulfate reduction processes are also suggested by the occurrence of pyrite framboids (Fig. 2b–d) within a calcite vein in sample 3881-1119 ($\delta^{34}S_{sulfide}$ of $-6.0‰$). Experimental studies demonstrate that pyrite framboids result from a spontaneous aggregation of colloidal suspension of greigite (Fe_3S_4; Wilkin and Barnes, 1997) and from FeS oxidation by H_2S (Butler and Rickard, 2000). However, Kohn et al. (1998) point out the importance of sulfate-reducing bacteria in their formation. They argue

that bacteria favor the precipitation of sulfide microcrystals, which may then form the pyrite framboids by the reaction of metal ions with dissolved sulfides on the cell walls of the bacteria (Fortin et al., 1997).

Samples H03-R2243 and H03-R2301, from the basement directly below the south face of the structure Poseidon (Fig. 1b), have distinctly high contents of mono- and disulfide-sulfur (of up to ~0.45 wt%) with high $\delta^{34}S$ values close to seawater sulfate ($\delta^{34}S_{disulfide}$ of +19.4‰ and +16.3‰, respectively; Fig. 4c and Table 3). Enrichment in ^{34}S and in sulfide-sulfur contents can occur during abiotic or biotic (closed-system) reduction of seawater sulfate. In a closed system, microbial sulfate reduction can be modeled as a Rayleigh fractionation process: as the sulfate remaining in solution is progressively enriched in ^{34}S, the dissolved sulfide produced by sulfate reduction will similarly be progressively enriched in ^{34}S. Thus, precipitation of sulfide produced from residual sulfate that has undergone significant sulfate reduction can explain these heavy sulfides. Similarly, microbial sulfate reduction in a closed-system has been inferred to explain the high $\delta^{34}S$ values of serpentinite samples recovered at 150 m depth in the drilled cores of Iberian Margin (Alt and Shanks, 1998).

Our results are consistent with microbiological studies on the Lost City vent material by Schrenk et al. (2004) and Brazelton et al. (2006). *Desulfotomaculum* species, which are known to be sulfate reducers (Imachi et al., 2006) and are common in high temperature and high pH environments (Reysenbach et al., 2002), were identified within the carbonate chimneys of the LCHF (Brazelton et al., 2006). Sulfate reducers are commonly associated with ANME-1, a group of anaerobic methane-oxidizing *Archaea* in anaerobic methane oxidation (AMO) environments. However, *Desulfotomaculum* species were identified in chimneys lacking ANME-1 and may be associated with other methane-cycling *Archaea*, such as the Lost City *Methanosarcinales* (LCMS) phylotype identified within the carbonate chimneys (Schrenk et al., 2004; Brazelton et al., 2006), or they may use H_2, CH_4, or hydrocarbons produced during serpentinization processes or the organic compounds present in the LCHF serpentinites as reducing agent (Stevens and McKinley, 1995; Delacour et al., 2008b).

Samples 3881-1119 and 3651-1252, which form the basement of active hydrothermal chimneys, display low $\delta^{34}S_{sulfate}$ values of −8.3‰ and +6.1‰ (Fig. 4a), respectively, and negative $\Delta^{34}S(SO_4^{2-} - FeS_2)$ of −4.6 and −2.3, respectively. These low $\delta^{34}S_{sulfate}$ values may be related to microbial sulfide oxidation processes in the basement. Under neutral to alkaline conditions, biotic sulfide oxidation, e.g., by the sulfide-oxidizing *Thiobacillus* species, produces a negative sulfate-sulfide fractionation of up to 15‰ (Toran and Harris, 1989) and leads to the formation of ^{34}S-depleted sulfates. The low $\delta^{34}S_{sulfate}$ values of samples 3881-1119 and 3651-1252 are consistent with this process (Fig. 4a). Elemental sulfur is a product of sulfide oxidation and is present in these two samples, while in low amounts (Table 3). Their $\delta^{34}S$ values of −5.3‰ and −5.7‰, respectively, are consistent with microbial sulfide oxidation and suggest concomitant formation with sulfate. Sulfide oxidizers belonging to the *Thiomicrospira* species and the epsilon-proteobacteria *Sulfurovum lithotrophicum* were identified in the carbonate chimneys and the hydrothermal fluids of the LCHF (Brazelton et al., 2006). Moreover, sulfur-cycling bacteria *Thermococcales* and *Crenarchaeota* are inferred to be present in the subsurface (Brazelton et al., 2006).

5.4. Sulfur geochemistry of the gabbros

The gabbros from the southern wall of the AM are characterized by a wide range of sulfur contents, a dominance of mono- and disulfides and only trace amounts of sulfates (Table 3 and Fig. 4a). Three of the analyzed gabbros (3639-1003, 3646-1138 and 3649-1257), distal to the LCHF (Fig. 1c), show bulk $\delta^{34}S$ values (−2.1‰ to −1.0‰, Fig. 8) in the range of oceanic gabbros and MORB, from −2‰ to +2‰ (Sakai et al., 1984; Alt et al., 1989; Alt and Anderson, 1991; Alt et al., 2007). Small variations in $\delta^{34}S$ can be attributed to magmatic differentiation (Thode et al., 1962; Shima et al., 1963; Sasaki, 1969a,b) or to speciation of sulfur in magma and separation or removal of sulfides from the silicate melt (Ueda and Sakai, 1984). The overall homogeneous sulfur isotope compositions of the AM gabbros, and their low sulfate concentrations, suggest that in general they were less affected by seawater alteration than the serpentinites (Delacour et al., 2008a).

A slight enrichment in ^{34}S in the monosulfides compared to disulfides, a low-sulfur content, and low $\delta^{34}S_{sulfate}$ values in sample 3649-1257 may indicate some local oxidation of the igneous sulfides by circulating seawater and/or incorporation of seawater-derived sulfides. The low $\delta^{34}S_{sulfate}$ values indicate a mixture of sulfates produced by oxidation of the monosulfides and seawater sulfate, similar to that observed at the Hess Deep, Iberian Margin, and MARK areas (Fig. 8; Alt and Shanks, 1998, 2003).

One oxide gabbro, sample 3880-1349, collected directly below the LCHF (Fig. 1b), shows the highest total sulfur content, with high sulfide- and sulfate-sulfur contents (Table 3). The elevated sulfide-sulfur content correlates with a high primary Fe_2O_3 concentrations (>25 wt%), and may reflect the increased solubility of sulfide in mafic melts with increasing total iron content (Haughton et al., 1974). Bulk rock, mono- and disulfides show enrichment in ^{34}S compared to mantle values, whereas the $\delta^{34}S$ values of the sulfates are low. This oxide gabbro is located close to the active portion of the hydrothermal system at Lost City and the high $\delta^{34}S$ values of the mono- and disulfides may be related to sulfide addition through hydrothermal alteration of subjacent gabbroic rocks at high temperature (~300–400 °C; Fig. 4c) and oxidation of the sulfide minerals by circulating seawater. Sulfates derived from oxidation of the sulfides mixed with seawater sulfates can explain the low $\delta^{34}S_{sulfate}$ values of sample 3880-1349.

5.5. Regional variability at the Atlantis Massif

The sulfur geochemistry of the basement rocks at the AM reveals a complex interplay of abiotic and biotic processes during its tectonic and alteration history. It is likely

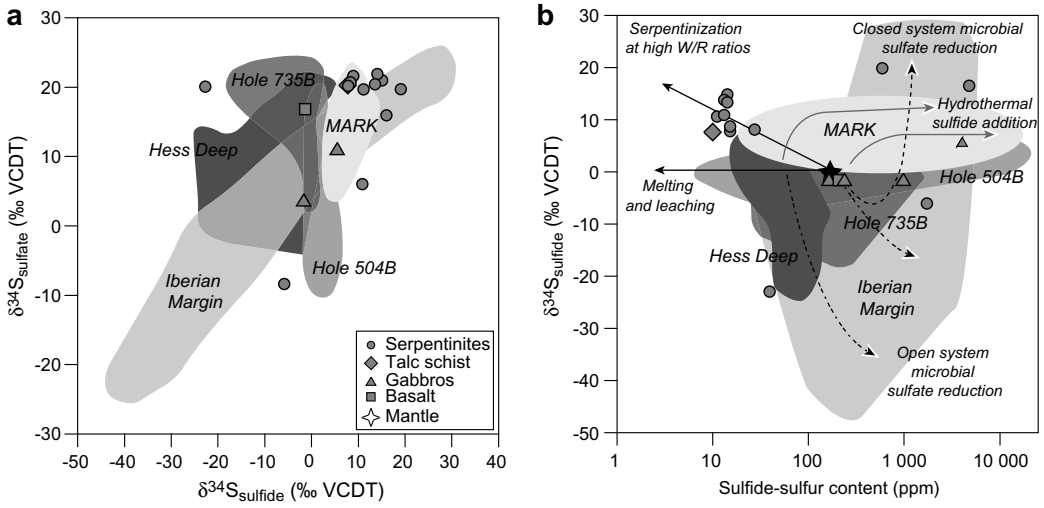

Fig. 8. Comparison of the serpentinites and gabbros of the southern AM-LCHF with serpentinized abyssal serpentinites and gabbros from other oceanic localities [Iberian margin and Hess Deep, Alt and Shanks (1998); Hole 735B, Alt and Anderson (1991); Hole 504B, Alt et al. (1989); and the MARK area, Alt and Shanks (2003)], showing: (a) $\delta^{34}S_{sulfate}$ plotted against $\delta^{34}S_{sulfide}$; and (b) $\delta^{34}S_{sulfide}$ plotted against sulfide-sulfur content. The serpentinites of the southern AM show the lowest sulfide-sulfur content associated with high $\delta^{34}S_{sulfide}$ values, reflecting a loss of sulfide and oxidation as major processes, consequences of the high fluid fluxes at the LCHF.

that close to the ridge axis, early serpentinization at low water–rock ratios and relatively high temperature took place under highly reducing conditions, leading to low-sulfur sulfide assemblages and precipitation of Fe–Ni alloys. However, pervasive long-lived serpentinization at high water–rock ratios and moderate temperatures has obliterated any original sulfur signatures in the AM peridotites, and has resulted in a net loss of sulfide-sulfur by oxidation and a gain of seawater sulfate.

Changes in the dominant, low- to moderate-temperature regime within the Lost City field influence sulfur speciation and sulfur isotope compositions of the basement rocks, carbonate chimneys and vent fluids, via inorganic and microbial processes. The presence of the sulfur-cycling bacteria *Thermococcales* and *Crenarchaeota* groups is inferred in the subseafloor beneath the field (Brazelton et al., 2006). These sulfur-metabolizing organisms likely use the hydrogen and methane in the hydrothermal fluids as reducing agent. Proskurowski et al. (2006) reported high concentrations of H_2 at the main carbonate structure Poseidon and a decrease in H_2 contents further away. Our studies are consistent with these results and indicate a spatial relationship between location and sulfur isotope compositions of the serpentinite samples. Sulfur isotope signatures that point to microbial processes were found only in serpentinites that were collected in basement rocks outcropping directly below the field. In particular, signatures indicating closed-system microbial sulfate reduction processes were found in the samples located directly beneath the 60 m tall tower Poseidon (Fig. 1b).

In addition to microbial processes, fluid flux is the dominant control on the redox conditions and sulfur geochemistry of the serpentinites and gabbros of the southern wall. High fluid fluxes produced higher fO_2 conditions, leading to sulfide oxidation and incorporation of seawater sulfate, likely as an adsorbed phase, in the basement rocks. A predominance of pyrite, indicative of higher fO_2 conditions, is only found in serpentinites and gabbros within the LCHF (Fig. 1b), whereas samples outside of the hydrothermal field (e.g., 3639-1055, 3639-1003, 3646-1138) are characterized by typical igneous sulfide assemblages (pyrrhotite, chalcopyrite and pentlandite) with negligible replacement by pyrite (e.g., 3649-1257).

Comparison of the serpentinites in the southern wall with serpentinized peridotites, olivine-rich troctolites and diverse gabbroic rocks recovered at the central dome of the AM at Hole 1309D reveal significant differences (Delacour et al., this issue). At the central dome, the serpentinites experienced addition of sulfides leached from hydrothermal alteration of the subjacent gabbroic rocks at high temperature and subsequent minor oxidation of the sulfide minerals. Downhole, the gabbroic rocks and olivine-rich troctolites have homogeneous mantle-like sulfur contents and sulfur isotope compositions with little variations related to magmatic variability or to interaction with fluids channeled in fault zones. In addition, the serpentinites, olivine-rich troctolites and olivine gabbros are dominated by Ni-rich and low-sulfur sulfide assemblages reflecting reducing conditions and limited seawater circulation at the central dome.

Sulfur geochemistry in serpentinite- and gabbro-hosted hydrothermal systems (Lost City, Iberian Margin, Hess Deep, MARK area, Logatchev) shows more variability than basalt-hosted black smoker hydrothermal systems (e.g., EPR, Hole 504B; Table 1). Because of the high temperatures of black smoker environments, inorganic sulfate reduction produces minor sulfur isotope fractionation and sulfides have similar $\delta^{34}S$ values as the parent sulfates (e.g., Ohmoto and Lasaga, 1982). Mixing of these sulfides with leached basaltic sulfur produces the limited range of $\delta^{34}S$ values observed in vent fluids and sulfide deposits (Table 1 and reference therein).

6. CONCLUSIONS

Sulfur geochemistry of basement rocks within the southern wall of the Atlantis Massif provides important constraints on seawater flux, alteration/serpentinization conditions, and the influence of microbial activity in an active peridotite-hosted hydrothermal system (Table 1 and Fig. 8). This study shows that the serpentinites and gabbros of the southern wall of the AM represent a more evolved system that has in general experienced higher fluid fluxes and more oxidizing conditions than most systems found to date (e.g., Iberian Margin; Agrinier et al., 1996; Alt and Shanks, 1998). High seawater fluxes and more pervasive serpentinization during the long-lived alteration history of the AM have obliterated early chemical signatures in the serpentinites and generated relatively high fO_2 conditions resulting in: a predominance of magnetite, the mobilization/dissolution and oxidation of the igneous sulfides to secondary pyrite, and incorporation of sulfates; all of which lead to high bulk $\delta^{34}S$ values. The dominance of oxidized sulfur species within the system may influence microbial diversity, which in turn influences the sulfur chemistry of the basement rocks.

The lack of anhydrite in the hydrothermal deposits at Lost City is most likely a result of present-day temperatures of <150 °C, consistent with vent fluid chemistry (Proskurowski et al., 2006) and microbiological studies (Brazelton et al., 2006). Sulfur isotopes in samples directly within the field reflect the influence of microbial activity in the subseafloor and below Poseidon (Brazelton et al., 2006), where the highest temperatures (90 °C) and the highest H_2 concentrations (15 mmol/kg) are found (Proskurowski et al., 2006). Temperatures and H_2 contents of the vent fluids decrease away from the main Poseidon structure, which together with fluid flow controlled by steeply dipping faults (Kelley et al., 2005; Karson et al., 2006) may influence the variations in sulfur isotope compositions.

A number of studies indicate that serpentinized peridotites are an important component of OCCs and may make up as much as 20–25% of the oceanic lithosphere at slow- and ultra-slow spreading ridges (e.g., Cannat et al., 1995; Smith et al., 2006; Dick et al., 2008; Smith et al., 2008). Our studies suggest that serpentinization processes and high seawater fluxes in uplifted serpentinized peridotites impart important changes in sulfur speciation and bulk sulfur isotope compositions of the oceanic lithosphere. These processes may influence the global sulfur cycle and consequently be important for mantle wedge compositions in subduction zones (Alt and Shanks, 2003). Subduction of a ^{34}S-enriched component, such as serpentinite-dominated oceanic crust with $\delta^{34}S$ values close to seawater, would lead to heterogeneities in sulfur contents and isotope compositions of mantle (Chaussidon et al., 1987) and subsequently would influence the sulfur isotope compositions of volcanic rocks to higher $\delta^{34}S$ values, as indicated from studies of basaltic rocks and mantle xenoliths in Germany (Harmon et al., 1987) and from volcanic rocks in island arcs (Ueda and Sakai, 1984; Woodhead et al., 1987).

ACKNOWLEDGEMENTS

We thank the captains, crews, and technical staffs aboard R/V *Atlantis* during cruises AT3-60 and AT7-34 to the Atlantis Massif in 2000 and 2003 for their tremendous support of this project. We also thank Chiara Boschi, Jeffrey Karson, Donna Blackman, and the *Atlantis* co-chiefs and scientific parties for their contributions to the data collection and discussions at sea. We acknowledge Maria Coray-Strasser, Luca Carrichi and Eric Reusser for assistance with the analyses. The authors appreciate the helpful comments of an anonymous reviewer and the previous associate editor Martin Goldhaber. We are particularly grateful for the extremely detailed and helpful comments of Jeff Alt, which led to a better understanding of this system and significantly improved our manuscript. The NOAA Ocean Exploration Program to Lost City and Bob Ballard provided additional samples and images of key outcrops. This work was supported by Swiss SNF Grants 2100-068055 and 200020-107620 to Früh-Green and Bernasconi and NSF Grant OCE-0426109 to Kelley.

REFERENCES

Agrinier P., Hekinian R., Bideau D. and Javoy M. (1995) O and H stable isotope compositions of oceanic crust and upper mantle rocks exposed in the Hess Deep near the Galapagos Triple Junction. *Earth Planet. Sci. Lett.* **136**, 183–196.

Agrinier P., Cornen G. and Beslier M.-O. (1996) Mineralogical and oxygen isotopic features of serpentinites recovered from the ocean-continent transition in the Iberia Abyssal Plain. In *Proceedings of the Ocean Drilling Program Scientific Results*, vol. 149 (eds. R. B. Whitmarsh, D. S. Sawyer, A. Klaus and D. G. Masson). pp. 541–552.

Allen D. E. and Seyfried W. E. J. (2004) Serpentinization and heat generation: constraints from Lost City and Rainbow hydrothermal systems. *Geochim. Cosmochim. Acta* **68**, 1347–1354.

Alt J. C. (1994) A sulfur isotopic profile through the Troodos ophiolite, Cyprus: primary composition and the effects of seawater hydrothermal alteration. *Geochim. Cosmochim. Acta* **58**, 1825–1840.

Alt J. C. and Anderson T. F. (1991) Mineralogy and isotopic composition of sulfur in Layer 3 gabbros from the Indian Ocean, Hole 735B. In *Proceedings of the Ocean Drilling Program Scientific Results*, vol. 118 (eds. R. P. Von Herzen and P. T. Robinson). Ocean Drilling Program, pp. 113–124.

Alt J. C. and Shanks W. C. (1998) Sulfur in serpentinized oceanic peridotites: serpentinization processes and microbial sulfate reduction. *J. Geophys. Res.* **103**, 9917–9929.

Alt J. C. and Shanks W. C. (2003) Serpentinization of abyssal peridotites from the MARK area, Mid-Atlantic Ridge: sulfur geochemistry and reaction modeling. *Geochim. Cosmochim. Acta* **67**, 641–653.

Alt J. C. and Shanks W. C. (2006) Stable isotope compositions of serpentinite seamounts in the Mariana forearc: serpentinization processes, fluid sources and sulfur metasomatism. *Earth Planet. Sci. Lett.* **242**, 272–285.

Alt J. C., Anderson T. F. and Bonnell L. (1989) The geochemistry of sulfur in a 1.3 km section of hydrothermally altered oceanic crust, DSDP Hole 504B. *Geochim. Cosmochim. Acta* **53**, 1011–1023.

Alt J. C., Shanks, III, W. C., Bach W., Paulick H., Garrido C. J. and Beaudoin G. (2007) Hydrothermal alteration and microbial sulfate reduction in peridotite and gabbro exposed by detachment faulting at the Mid-Atlantic Ridge, 15° 20′N (ODP Leg 209): a sulfur and oxygen isotope study. *Geochem. Geophys. Geosyst.* **8**, Q08002. doi:10.1029/2007GC001617.

Andrews A. J. (1979) On the effect of low-temperature seawater–basalt interaction on the distribution of sulfur in oceanic crust, layer 2. *Earth Planet. Sci. Lett.* **46**, 68–80.

Arnold M. and Sheppard S. M. F. (1981) East Pacific Rise at latitude 21°N: isotopic composition and origin of the hydrothermal sulfur. *Earth Planet. Sci. Lett.* **56**, 148–159.

Bach W., Garrido C. J., Paulick H., Harvey J. and Rosner M. (2004) Seawater-peridotite interactions: first insights from ODP Leg 209, MAR 15°N. *Geochem. Geophys. Geosyst.* **5**, Q09F26. doi:10.1029/2004GC000744.

Baker E. T. and German C. (2004) On the global distribution of mid-ocean ridge hydrothermal vent-fields. In *Mid-ocean ridges: hydrothermal interactions between the lithosphere and oceans*, vol. 148 (eds. C. R. German, J. Lin and L. M. Parson). American Geophysical Union, Washington, DC, pp. 245–266.

Blackman D. K., Cann J. R., Jannsen B. and Smith D. K. (1998) Origin of extensional core complexes: evidences from the Mid-Atlantic Ridge at Atlantis Fracture Zone. *J. Geophys. Res.* **103**, 21315–21333.

Blackman D. K., Karson J. A., Kelley D. S., Cann J. R., Früh-Green G., Gee J. S., Hurst S. D., John B. E., Morgan J., Nooner S. L., Kent Ross D., Schroeder T. J. and Williams E. A. (2002) Geology of the Atlantis Massif (Mid-Atlantic Ridge, 30°N): implications for the evolution of an ultramafic oceanic core complex. *Mar. Geophys. Res.* **23**, 443–469.

Blackman D. K., Ildefonse B., John B. E., Ohara Y., Miller D. J., MacLeod C. J. and the Expedition 304/305 Scientists (2006) In *Proceedings Integrated Ocean Drilling Program, 304/305*. College Station TX (Integrated Ocean Drilling Program Management International, Inc.). doi:doi:10.2204/iodp.proc.304305.2006.

Boetius A. (2005) The Lost City life. *Science* **307**, 1420–1422.

Boetius A., Ravenschlag K., Schubert C. J., Rickert D., Widdel F., Gieseke A., Amann R., Jorgensen B. B., Witte U. and Pfannkuche O. (2000) A marine microbial consortium apparently mediating anaerobic oxidation of methane. *Nature* **407**, 623–626.

Bogdanov Y. A., Bortnikov N. S. and Sagalevitch A. M. (1997) New type of the modern forming system: black smokers of the hydrothermal field 14° 45′N, MAR. *Geol. Ore Deposits* **39**, 68–90.

Boschi C. (2006) Building Lost City: serpentinization, mass transfer, and fluid flow in an oceanic core complex. Ph.D. Thesis No. 16720, ETH Zürich.

Boschi C., Früh-Green G. L., Delacour A., Karson J. A. and Kelley D. S. (2006) Mass transfer and fluid flow during detachment faulting and development of an oceanic core complex, Atlantis Massif (MAR 30°N). *Geochem. Geophys. Geosyst.* **7**, Q01004. doi:10.1029/2005GC001074.

Boschi C., Dini A., Früh-Green G. L. and Kelley D. S. (2008) Isotopic and element exchange during serpentinization and metasomatism at the Atlantis Massif: insights from B and Sr isotopes. *Geochim. Cosmochim. Acta* **72**, 1801–1823. doi:10.1016/j.gca.2008.01.013.

Brazelton W. J., Schrenk M. O., Kelley D. S. and Baross J. A. (2006) Methane- and sulfur-metabolizing microbial communities dominate the Lost City Hydrothermal Field ecosystem. *Appl. Environ. Microbiol.* **72**, 6257–6270.

Brunner B. and Bernasconi S. M. (2005) A revised isotope fractionation model for dissimilatory sulfate reduction in sulfate reducing bacteria. *Geochim. Cosmochim. Acta* **69**, 4759–4771.

Brunner B., Yu J. Y., Mielke R. E., MacAskill J. A., Madzunkov S., McGenity T. J. and Coleman M. (2008) Different isotope and chemical patterns of pyrite oxidation related to lag and exponential growth phases of *Acidithiobacillus ferrooxidans* reveal a microbial growth strategy. *Earth Planet. Sci. Lett.* **270**, 63–72.

Butler I. B. and Rickard D. (2000) Framboidal pyrite formation via the oxidation of iron (II) monosulfide by hydrogen sulphide. *Geochim. Cosmochim. Acta* **64**, 2665–2672.

Cannat M., Mével C., Maia M., Deplus C., Durand C., Gente P., Agrinier P., Belarouchi A., Dubuisson G., Humler E. and Reynolds J. (1995) Thin crust, ultramafic exposures, and rugged fault patterns at the Mid-Atlantic Ridge (22°–24°N). *Geology* **23**, 49–52.

Cann J. R., Blackman D. K., Smith D. K., McAllister E., Janssen B., Mello S., Avgerinos E., Pascoe A. R. and Escartin J. (1997) Corrugated slip surfaces formed at ridge-transform intersections on the Mid-Atlantic Ridge. *Nature* **385**, 329–332.

Charlou J. L., Donval J. P., Fouquet Y., Jean-Baptiste P. and Holm N. (2002) Geochemistry of high H_2 and CH_4 vent fluids issuing from ultramafic rocks at the Rainbow hydrothermal field (36° 14′N, MAR). *Chem. Geol.* **191**, 345–359.

Chaussidon M., Albarède F. and Sheppard S. M. F. (1987) Sulphur isotope heterogeneity in the mantle from ion microprobe measurement of sulphide inclusions in diamonds. *Nature* **330**, 242–244.

Chiba H., Uchiyama N. and Teagle D. A. H. (1998) Stable isotope study of anhydrite and sulfide minerals at the TAG hydrothermal mound, Mid-Atlantic Ridge, 26°N. In *Proceedings of Ocean Drilling Program Scientific Results*, vol. 158 (eds. P. M. Herzig, S. E. Humphris and D. J. Miller). Ocean Drilling Program, pp. 85–90.

Delacour A., Früh-Green G. L., Bernasconi S. M. and Kelley D. S. (2005) The influence of high seawater fluxes on sulfur compositions of the serpentinized peridotites at the Lost City Hydrothermal Field. *EOS Trans. AGU* **86**(52), Fall Meet. Suppl., V51B-1488 (abstr.).

Delacour, A., Früh-Green G. L., Bernasconi S. M. (this issue) Sulfur mineralogy and geochemistry of serpentinites and gabbros of the Atlantis Massif (IODP Site U1309). *Geochim. Cosmochim. Acta.*, doi:10.1016/j.gca.2008.07.018.

Delacour A., Früh-Green G. L., Frank M., Gutjahr M. and Kelley D. S. (2008a) Sr- and Nd-isotope geochemistry of the Atlantis Massif (30°N, MAR): implications for fluid fluxes and lithospheric heterogeneity. *Chem. Geol.* **254**, 19–35. doi:10.1016/j.chemgeo.2008.05.018.

Delacour A., Früh-Green G. L., Bernasconi S. M., Schaeffer P. and Kelley D. S. (2008b) Carbon geochemistry of serpentinites in the Lost City hydrothermal system. *Geochim. Cosmochim. Acta.* **72**, 3681–3702. doi:10.1016/j.gca.2008.04.039.

Dick H. J. B., Tivey M. A. and Tucholke B. (2008) Plutonic foundation of a slow-ridge segment: oceanic core complex at Kane Megamullion, 23° 30′N, 45° 20′W. *Geochem. Geophys. Geosyst.* **9**, Q05014. doi:10.1029/2007GC001645.

Donval J. P., Charlou J.-L., Douville E., Knoery E. and Fouquet Y. (1997) High H_2 and CH_4 content in hydrothermal fluids from Rainbow site newly samples at 36° 14′N on the AMAR segment, Mid-Atlantic Ridge (diving FLORES cruise, July 1997). Comparisons with other MAR dives. *EOS Trans. AGU* **78**, 832.

Douville E., Charlou J. L., Donval J. P., Knoery J. and Fouquet Y. (1997) Trace elements in fluids from the new Rainbow hydrothermal field (36°14 N, MAR): a comparison with other Mid-Atlantic Ridge fluids. *EOS Trans. AGU* **78**, 832.

Duckworth R. C., Knott R., Fallick A. E., Rockard D., Murton B. J. and Dover C. J. (1995) Mineralogy and sulphur isotope geochemistry of the Broken Spur sulfides, 29°N, Mid-Altantic Ridge. In *Hydrothermal Vents and Processes*, vol. 87 (eds. L. M. Parson, C. L. Walker and D. R. Dixon). Geological Society Special Publication, pp. 175–189.

Eckstrand O. R. (1975) The Dumont serpentinite: a model for control of nickeliferous opaque mineral assemblages by alteration reactions in ultramafic rocks. *Econ. Geol.* **70**, 183–201.

Eickmann B., Strauss H., Koschinsky A., Kuhn T., Petersen S. and Schmidt K. (2005) Sulphur cycling at the Mid-Atlantic Ridge: isotopic evidence from the Logatchev and Turtle Pits Hydrothermal Fields. *EOS Trans. AGU* **86**(52), Fall Meeting, OS22A-01 (abstr.).

Eickmann B., Peters M., Strauss H., Koschinsky A., Kuhn T., Petersen S. and Schmidt K. (2006) Isotopic evidence for sulphur cycling at the Mid-Atlantic Ridge. *Geophys. Res.* EGU06-A-07252 (abstr.).

Expedition Scientific Party (2005a) Oceanic core complex formation, Atlantis Massif, *IODP Prel. Rept., 304*. Available from: <http://iodp.tamu.edu/publications/PR/304PR/304PR.PDF>.

Expedition Scientific Party (2005b) Oceanic core complex formation, Atlantis Massif, *IODP Prel. Rept., 305*. Available from: <http://iodp.tamu.edu/publications/PR/305PR/305PR.PDF>.

Farrand M. (1970) Framboidal sulphides precipitated synthetically. *Mineral. Deposita* **5**, 237–247.

Fortin D., Ferris F. G. and Beveridge T. J. (1997) Surface-mediated mineral development by bacteria. In *Geomicrobiology: Interactions Between Microbes and Minerals*, vol. 35 (eds. J. F. Banfield and K. H. Nealson). Mineralogical Society of America, pp. 161–180.

Frost B. R. (1985) On the stability of sulfides, oxides, and native metals in serpentinite. *J. Petrol.* **26**, 31–63.

Früh-Green G. L., Boschi C., Kelley D. S., Connelly J. A. D. and Schrenk M. O. (2002) The role of serpentinization in metasomatism, carbonate precipitation, and microbial activity: Stable isotope constraints from the Lost City Vent Field (MAR, 30°N). *EOS Trans. AGU* **83**(47), Fall Meet. Suppl., V72A-1289 (abstr.).

Früh-Green G. L., Kelley D. S., Bernasconi S. M., Karson J. A., Ludwig K. A., Butterfield D. A., Boschi C. and Proskurowski G. (2003) 30,000 years of hydrothermal activity at the Lost City Vent Field. *Science* **301**, 495–498.

Früh-Green G. L., Connolly J. A. D., Plas A., Kelley D. S. and Grobéty B. (2004) Serpentinization of oceanic peridotites: implications for geochemical cycles and biological activity. In *The Subseafloor Biosphere at Mid-Ocean Ridges*, vol. 144 (eds. W. S. D. Wilcock, E. F. DeLong, D. S. Kelley, J. A. Baross and S. C. Cary). American Geophysical Union, Washington DC, pp. 119–136.

Fry B., Ruf W., Gest H. and Hayes J. M. (1988) Sulfur isotope effects associated with oxidation of sulfide by O_2 in aqueous solution. *Chem. Geol.* **73**, 205–210.

Geeldhoed J. S., Hiemstra T. and Van Riemsdijk W. H. (1997) Phosphate and sulfate adsorption on goethite: single anion and competitive adsorption. *Geochim. Cosmochim. Acta.* **61**, 2389–2396.

Gellatly A. M. and Lyons T. W. (2005) Trace sulfate in mid-Proterozoic carbonates and the sulfur isotope record of biospheric evolution. *Geochim. Cosmochim. Acta.* **69**, 3813–3829.

Gemmel J. B. and Sharpe R. (1998) Detailed sulfur-isotope investigation of the TAG hydrothermal mound and stockwork zone, 26°N, Mid-Atlantic Ridge. In *Proceedings of Ocean Drilling Program*, vol. 158 (eds. P. M. Herzig, S. E. Humphris, D. J. Miller and R. A. Zierenberg). Ocean Drilling Program, pp. 71–84.

German C. and Von Damm K. L. (2003) Hydrothermal processes. In *Treatise on Geochemistry*, vol. 6 (eds. H. Elderfield, H. D. Holland and K. K. Turekian). Elsevier, pp. 181–222.

Gitlin E. (1985) Sulfide remobilization during low temperature alteration of seafloor basalt. *Geochim. Cosmochim. Acta.* **49**, 1567–1579.

Goldhaber M. B. (1983) Experimental study of metastable sulfur oxyanion formation during pyrite oxidation at pH 6–9 and 30 °C. *Am. J. Sci.* **283**, 193–217.

Goldhaber M. B. and Kaplan I. R. (1980) Mechanisms of sulfur incorporation and isotope fractionation during early diagenesis in sediments of the Gulf of California. *Mar. Chem.* **9**, 95–143.

Goldhaber M. B. and Orr W. L. (1995) Kinetic controls on thermochemical sulfate reduction as a source of sedimentary H_2S. In *Geochemical Transformations of Sedimentary Sulfur*, vol. 612 (eds. M. A. Vairavamurthy, M. A. A. Schoonen, T. I. Eglinton, G. W. Luther and B. Manowitz). American Chemical Society, pp. 412–425.

Grinenko V. A. and Mineyev S. D. (1992) Low-temperature leaching of sulfur from basic rocks. *Geochem. International* **29**, 77–91.

Harmon R. S., Hoefs J. and Wedepohl K. H. (1987) Stable isotope (O, H, S) relationships in tertiary basalts and their mantle xenoliths for the Northern Hessian Depression, W. Germany. *Contrib. Mineral. Petrol.* **95**, 350–369.

Hartman G. and Wedepohl K. H. (1993) The composition of peridotite tectonites from the Ivrea Complex, northern Italy: residues from melt extraction. *Geochim. Cosmochim. Acta* **57**, 1761–1782.

Haughton D. R., Roeder P. L. and Skinner B. J. (1974) Solubility of sulfur in mafic magmas. *Econ. Geol.* **69**, 451–467.

Holm N. and Charlou J.-L. (2001) Initial indications of abiotic formation of hydrocarbons in the Rainbow ultramamafic hydrothermal system, Mid-Atlantic Ridge. *Earth Planet. Sci. Lett.* **191**, 1–8.

Ildefonse B., Blackman D., John B. E., Ohara Y., Miller D. J. and MacLeod C. J.and IODP Expeditions 304/305 Science Party (2007) Oceanic core complexes and crustal accretion at slow-spreading ridges. *Geology* **35**, 623–626.

Imachi H., Sekiguchi Y., Kamagata Y., Loy A., Qiu Y.-L., Hugenholtz P., Kimura N., Wagner M., Ohashi A. and Harada H. (2006) Non-sulfate reducing bacteria, syntrophic bacteria affiliated with *Desulfotomaculum* cluster I are widely distributed in methanogenic environments. *Appl. Environ. Microbiol.* **72**, 2080–2091.

Inskeep W. P. (1989) Adsorption of sulfate by kaolinite and amorphous iron oxide in the presence of organic ligands. *J. Environ. Qual.* **18**, 379–385.

Janecky D. R. and Seyfried W. E. J. (1986) Hydrothermal serpentinization of peridotite within the oceanic crust: experimental investigations of mineralogy and major element chemistry. *Geochim. Cosmochim. Acta* **50**, 1357–1378.

Karson J. A., Früh-Green G., Kelley D. S., Williams E. A., Yoerger D. R. and Jakuba M. (2006) Detachment shear zone of the Atlantis Massif core complex, Mid-Atlantic Ridge, 30°N. *Geochem. Geophys. Geosyst* **7**, Q06016. doi:10.1029/2005GC001109.

Kase K., Yamamoto M. and Shibata T. (1990) Copper-rich sulfide deposits near 23°N, Mid-Atlantic Ridge: chemical composition, mineral chemistry and sulfur isotopes. In *Proceedings of Ocean Drilling Program*, vol. 106/109 (eds. R. Detrick, J. Honnorez, W. B. Bryan and T. Juteau). Ocean Drilling Program, pp. 163–173.

Kelley D. S., Karson J. K., Blackam D. K., Früh-Green G. L., Butterfield D. A., Lilley M. D., Olson E. J., Schrenk M. O., Roe K. K., Lebon G. T. and Rivizzigno P. and Scientific Party (2001) An off-axis hydrothermal vent field near the Mid-Atlantic Ridge at 30°N. *Nature* **412**, 145–149.

Kelley D. S., Karson J. A., Früh-Green G. L., Yoerger D. R., Shank T. M., Butterfield D. A., Hayes J. M., Schrenk M. O., Olson E. J., Proskurowski G., Jakuba M., Bradley A., Larson B., Ludwig K., Glickson D., Buckman K., Bradley A. S., Brazelton W. J., Roe K., Elend M. J., Delacour A., Bernasconi S. M., Lilley M. D., Baross J. A., Summons R. E. and Sylva S. (2005) A serpentinite-hosted ecosystem: the Lost City Hydrothermal Field. *Science* **307**, 1428–1434.

Kerridge J. F., Haymon R. M. and Kastner M. (1983) Sulfur isotope systematics at the 21°N site, East Pacific Rise. *Earth Planet. Sci. Lett.* **66**, 91–100.

Knott R., Fallick A. E., Richards K. J. and Bäcker H. (1995) Mineralogical and sulphur isotope characteristics of a massive sulfide boulder, Galapagos Rift, 85° 55′W. In *Hydrothermal Vents and Processes*, vol. 87 (eds. L. M. Parson, C. L. Walker and D. R. Dixon). Geological Society Special Publication, pp. 207–222.

Knott R., Fouquet Y., Honnorez J., Petersen S. and Bohn M. (1998) Petrology and hydrothermal mineralization: a vertical section through the TAG mound. In *Proceedings of Ocean Drilling Program*, vol. 158 (eds. P. M. Herzig, S. E. Humphris, D. J. Miller and R. A. Zierenberg). Ocean Drilling Program, pp. 5–26.

Kohn M. J., Riciputi L. R., Stakes D. and Orange D. L. (1998) Sulfur isotope variability in biogenic pyrite: reflections of heterogeneous bacterial colonization? *Am. Mineral.* **83**, 1454–1468.

Krasnov S. G., Cherkashov G. A. and Stepanova T. V. (1995) Detailed geological studies of hydrothermal fields in the North Atlantic. In *Hydrothermal Vents and Processes*, vol. 87 (eds. L. M. Parson, C. L. Walker and D. R. Dixon). Geological Society Special Publication, pp. 43–64.

Kusukabe M., Mayeda S. and Nakamura E. (1990) S, O and Sr isotope systematics of active vent materials from the Mariana backarc basin spreading axis at 18°N. *Earth Planet. Sci. Lett.* **100**, 275–282.

Lorand J.-P. (1991) Sulphide petrology and sulphur geochemistry of orogenic lherzolites: a comparitive study of the Pyrenean bodies (France) and the Lanzo Massif (Italy). In *Orogenic Lherzolites and Mantle Processes* (ed. M. A. Menzies). Oxford University Press, pp. 77–95.

Lowell R. P. and Rona P. A. (2002) Seafloor hydrothermal systems driven by the serpentinization of peridotite. *Geophys. Res. Lett.* **29**, 1–4. doi:10.1029/2001GL014411.

Ludwig K., Kelley D. S., Butterfield D. A., Nelson B. K. and Früh-Green G. L. (2006) Formation and evolution of carbonate chimneys at the Lost City Hydrothermal Field. *Geochim. Cosmochim. Acta* **70**, 3625–3645.

Machel H. G., Krouse H. R. and Sassen R. (1995) Products and distinguishing criteria of bacterial and thermochemical sulfate reduction. *Appl. Geochem.* **10**, 373–389.

Mottl M. J., Holland H. D. and Corr R. F. (1979) Chemical exchange during hydrothermal alteration of basalt by seawater. II. Experimental results for Fe, Mn, and sulfur species. *Geochim. Cosmochim. Acta* **43**, 869–884.

Ohmoto H. and Goldhaber M. B. (1997) Sulfur and carbon isotopes. In *Geochemistry of Hydrothermal Ore Deposits* (ed. H. L. Barnes), 3rd edition. Wiley, pp. 517–611.

Ohmoto H. and Lasaga A. C. (1982) Kinetics of reactions between aqueous sulfates and sulfides in hydrothermal systems. *Geochim. Cosmochim. Acta* **46**, 1727–1745.

Ohmoto H. and Rye R. O. (1979) Isotopes of sulfur and carbon. In *Geochemistry of Hydrothermal Ore Deposits* (ed. H. L. Barnes). pp. 509–567.

Palandri J. L. and Reed M. H. (2004) Geochemical models of metasomatism in ultramafic systems: serpentinization, rodingitization, and seafloor carbonate chimney precipitation. *Geochim. Cosmochim. Acta* **68**, 1115–1133.

Pisapia C., Chaussidon M., Mustin C. and Humbert B. (2007) O and S isotopic composition of dissolved and attached oxidation products of pyrite by *Acidithiobacillus ferrooxidans*: comparison with abiotic oxidations. *Geochim. Cosmochim. Acta* **71**, 2474–2490.

Proskurowski G., Lilley M. D., Kelley D. S. and Olson E. J. (2006) Low temperature volatile production at the Lost City Hydrothermal Field, evidence from a hydrogen stable isotope geothermometer. *Chem. Geol.* **229**, 331–343.

Proskurowski G., Lilley M. D., Seewald J. S., Früh-Green G. L., Olson E. J., Lupton J. E., Sylva S. P. and Kelley D. S. (2008) Abiogenic hydrocarbon production at Lost City Hydrothermal Field. *Science* **319**, 604–607.

Rees C. E., Jenkyns H. C. and Monster J. (1978) The sulphur isotopic composition of ocean water sulphate. *Geochim. Cosmochim. Acta* **42**, 377–382.

Reysenbach A. L., Gotz D. and Yernool D. (2002) Microbial diversity of marine and terrestrial thermal springs. In *Biodiversity of Microbial Life* (eds. J. T. Staley and A. L. Reysenbach). Wiley-Liss Inc, pp. 345–421.

Ringwood A. E. (1966) The chemical composition and origin of the earth. In *Advances in Earth Sciences* (ed. P. M. Hurley). MIT Press, pp. 287–356.

Rona P. A., Widenfalk L. and Bostrom K. (1987) Serpentinized ultramafics and hydrothermal activity at the Mid-Atlantic Ridge crest near 15°N. *J. Geophys. Res.* **92**, 1417–1427.

Rouxel O., Fouquet Y. and Ludden J. N. (2004) Subsurface processes at the Lucky Strike hydrothermal field, Mid-Atlantic Ridge: evidence from sulfur, selenium, and iron isotopes. *Geochim. Cosmochim. Acta* **68**, 2295–2311.

Sagalevich A. M., Vinogradov G. M., Gurivich E. G., Lein A. Y., Lukashin V. N. and Chernyaev E. S. (2000) Investigations in the Titanic study area and the Rainbow Hydrothermal Field in Cruise 42 of the Research Vessel Akademik Mstislav Keldysh. *Oceanology* **40**, 439–446.

Sakai H., Des Marais D. J., Ueda A. and Moore J. G. (1984) Concentrations and isotope ratios of carbon, nitrogen and sulfur in ocean-floor basalts. *Geochim. Cosmochim. Acta* **48**, 2433–2441.

Sasaki A. (1969a) Sulfur isotope variations in Skaergaard rocks. *Geol. Soc. Am. Spec. Pap.* **121**, 263–264.

Sasaki A. (1969b) Sulphur isotope study of the Muskox intrusion, district of Mackenzie. *Geol. Surv. Can. Pap.*, 1–68.

Schoonen M. A. A. and Barnes H. L. (1991) Reactions forming pyrite and marcasite from solution: II. Via FeS precursors below 100 °C. *Geochim. Cosmochim. Acta* **55**, 1505–1514.

Schrenk M. O., Kelley D. S., Bolton S. A. and Baross J. A. (2004) Low Archaeal diversity linked to subseafloor geochemical processes at the Lost City Hydrothermal Field, Mid-Atlantic Ridge. *Environ. Microbiol.* **6**, 1086–1095.

Schroeder T. and John B. E. (2004) Strain localization on an oceanic detachment fault system, Atlantis Massif, 30°N, Mid-Atlantic Ridge. *Geochem. Geophys. Geosyst.* **5**. doi:10.1029/2004GC000728.

Seyfried W. E. J. and Dibble W. E. J. (1980) Seawater-peridotite interaction at 300 °C and 500 bars; implications for the origin of oceanic serpentinites. *Geochim. Cosmochim. Acta* **44**, 309–322.

Shanks W. C. (2003) Stable isotope in seafloor hydrothermal systems. In *Stable Isotope Geochemistry*, vol. 43 (eds. J. W. Valley and D. R. Cole). Reviews in Mineralogy and Geochemistry. Mineralogical Society of America, pp. 469–525.

Shanks, III, W. C. and Seyfried W. E. J. (1987) Stable isotope studies of vent fluids and chimneys minerals, Southern Juan de

Fuca Ridge: sodium metasomatism and seawater sulfate reduction. *J. Geophys. Res.* **92**, 11387–11399.

Shanks, III, W. C., Bohlke J. K. and Seal, II, R. R. (1995) Stable isotopes in mid-ocean ridge hydrothermal systems: interactions between fluids, minerals, and organisms. In *Seafloor Hydrothermal Systems: Physical, Chemical, Biological, and Geological interactions*, vol. 70 (eds. S. E. Humphris, R. A Zierenberg, L. S. Mullineaux and R. E. Thomson). American Geophysical Union, Washington DC, pp. 194–221.

Shima M., Gross W. H. and Thode H. G. (1963) Sulfur isotope abundance in basic sills, differentiated granites and meteorites. *J. Geophys. Res.* **68**, 2835–2847.

Skirrow R. and Coleman M. L. (1982) Origin of sulfur and geothermometry of hydrothermal deposits from the Galapagos Rift, 86°W. *Nature* **299**, 142–144.

Smith D. K., Cann J. R. and Escartin J. (2006) Widespread active detachment faulting and core complex formation near 13°N on the Mid-Atlantic Ridge. *Nature* **442**, 440–443.

Smith D. K., Escartin J., Schouten H. and Cann J. R. (2008) Fault rotation and core complex formation: significant processes in seafloor formation at slow-spreading mid-ocean ridges (Mid-Atlantic Ridge, 13 –15°N). *Geochem. Geophys. Geosyst.* **9**. doi:10.1029/2007GC001699.

Stetter K. O. (1996) Hyperthermophilic prokaryotes. *FEMS Microbiol. Rev.* **18**, 149–158.

Stevens T. O. and McKinley J. P. (1995) Lithoautotrophic microbial ecosystems in deep basalt aquifers. *Science* **270**, 450–454.

Studley S. A., Ripley E. M., Elswick E. R., Dorais M. J., Fong J., Finkelstein D. and Pratt L. M. (2002) Analysis of sulfides in whole rock matrices by elemental analyzer—continuous flow isotope ratio mass spectrometry. *Chem. Geol.* **192**, 141–148.

Styrt M. M., Brackmann A. J., Holland H. D., Clark B. C., Pisutha-Arnond V., Eldridge C. S. and Ohmoto H. (1981) The mineralogy and the isotopic composition of sulfur in hydrothermal sulfide/sulfate deposits on the East Pacific Rise, 21°N latitude. *Earth Planet. Sci. Lett.* **53**, 382–390.

Thode H. G., Dunford H. B. and Shima M. (1962) A thermodynamic study of pyrite and pyrrhotite. *Geochim. Cosmochim. Acta* **28**, 641–671.

Toran L. and Harris R. F. (1989) Interpretation of sulfur and oxygen isotopes in biological and abiological sulfide oxidation. *Geochim. Cosmochim. Acta* **53**, 2341–2348.

Tuttle M. L., Goldhaber M. B. and Williamson D. L. (1986) An analytical scheme for determining forms of sulphur in oil shales and associated rocks. *Talanta* **33**, 953–961.

Ueda A. and Sakai H. (1984) Sulfur isotope study of Quaternary volcanic rocks from Japanese Islands Arc. *Geochim. Cosmochim. Acta* **48**, 1837–1848.

Wilkin R. T. and Barnes H. L. (1997) Formation processes of framboidal pyrite. *Geochim. Cosmochim. Acta* **61**, 323–339.

Woodhead J. D., Harmon R. S. and Fraser D. G. (1987) O, S, Sr, and Pb isotope variations in volcanic rocks from the northern Mariana Islands: implication for crustal recycling in intra-oceanic arcs. *Earth Planet. Sci. Lett.* **83**, 39–52.

Associate editor: Jeffrey C. Alt